Title
Rare earth element systematics in boiled fluids from basalt-hosted geothermal systems

Permalink
https://escholarship.org/uc/item/4687r8sd

Authors
Fowler, Andrew PG
Zierenberg, Robert A
Reed, Mark H
et al.

Publication Date
2019

DOI
10.1016/j.gca.2018.10.001

Peer reviewed

Rare earth element systematics in boiled fluids from basalt-hosted geothermal systems

Andrew P.G. Fowler [a,1,*], Robert A. Zierenberg [a], Mark H. Reed [b], James Palandri [b], Finnbogi Óskarsson [c], Ingvi Gunnarsson [d]

[a] *Department of Earth and Planetary Sciences, University of California, Davis, CA 95616, USA*
[b] *Department of Geological Sciences, University of Oregon, Eugene, OR 97403, USA*
[c] *Iceland GeoSurvey, Grensásvegur 9, 108 Reykjavík, Iceland*
[d] *Reykjavík Energy, Bæjarhálsi 1, 110 Reykjavík, Iceland*

Abstract

Hydrothermal processes that lead to REE fractionation and redistribution are important for understanding water-rock interactions in geothermal energy resources and mineral deposits, and for determining how submarine hydrothermal activity affects the composition of oceanic crust. Much previous work on REE transport and deposition has focused on submarine hydrothermal vents. We report REE concentrations in boiled fluids sampled from five subaerial, basalt-hosted geothermal fields, and explore controls on aqueous REE concentrations by ligand complexation and mineral supersaturation. Samples that boiled at pressures between 0.8 and 2.83 MPa were obtained from the Reykjanes, Svartsengi, Hellisheidi, and Nesjavellir geothermal systems in Iceland, and the Puna geothermal system in Hawaii. For comparison, we also report REE concentrations in hydrothermal fluids from the sediment hosted submarine Middle Valley hydrothermal system, which boiled at >250 MPa. The $pH_{(25°C)}$ values of the sampled subaerial geothermal fluids range from 3.94 to 6.77, and Cl concentrations range from near seawater (502 mmol/kg) to dilute (1.9 mmol/kg). La, Ce and Eu are the only REE present at levels above 5 picomole/kg (pmol/kg) in the boiled geothermal fluids; and there are notable CI chondrite normalized La and Eu anomalies in the saline fluids. REE concentrations in Middle Valley hydrothermal fluids fall within the typical range reported for submarine hydrothermal fluids and have around two orders of magnitude higher REE than the boiled subaerial geothermal fluids. Bulk samples of precipitates in pipes from the Reykjanes geothermal system have detectable REE, confirming that downhole fluids have lost REE during boiling and production of fluids for geothermal energy. Isenthalpic boiling models show that the proportions of La and Eu chloride complexes increase relative to other aqueous species as boiling progresses, attenuating the incorporation of La and Eu into precipitated well scale solids. Fluorapatite is calculated to precipitate on boiling of low pH and saline fluids and calcite is calculated to precipitate from dilute and near-neutral pH fluids, and these minerals likely sequester REE in boiled subaerial fluids. Submarine hydrothermal fluids are constrained to boiling at higher temperatures than subaerial geothermal fluids owing to pressure from overlying cold seawater, therefore secondary minerals and solids that incorporate REE are not extensively precipitated and REE concentrations in the fluids are higher.
© 2018 Elsevier Ltd. All rights reserved.

Keywords: Rare earth elements; Boiling, Geothermal; Hydrothermal; Geochemical modeling; Aqueous speciation; Apatite partitioning

* Corresponding author.
 E-mail address: afowler@umn.edu (A.P.G. Fowler).
[1] Presently at the Department of Earth Sciences, University of Minnesota, Minneapolis, CA 55455, USA.

1. INTRODUCTION

Rare earth element (REE; La through Lu) abundances in fluids and secondary minerals provide information about geochemical processes operating along fluid flow paths in the subsurface hosting subaerial geothermal energy resources and submarine hydrothermal systems, locations that are challenging to sample directly (Craddock et al., 2010; Humphris and Bach, 2005; Möller et al., 2003; Möller et al., 2008; Sanada et al., 2006; van Middlesworth and Wood, 1997; Wheat et al., 2002). Hydrothermal controls on REE solubility can lead to enrichment of REE to economically important levels, and are important for understanding the formation of many REE mineral deposits (Lottermoser, 1992; Williams-Jones et al., 2012).

Many studies on hydrothermal REE mobility have focused on basalt-hosted submarine hydrothermal systems. The REE_N (subscript N is used to denote the CI chondrite normalized concentration in the present work) pattern of submarine hydrothermal fluids from around the globe are remarkably similar with large positive Eu anomalies and LREE (Light REE; La through Eu) enrichment relative to HREE (Heavy REE; Gd through Lu), albeit absolute REE concentrations vary over several orders of magnitude (Campbell et al., 1988; Douville et al., 1999; Klinkhammer et al., 1994; Michard et al., 1983; Mitra et al., 1994). REE patterns in submarine hydrothermal fluids have been attributed to dissolution of igneous plagioclase in the host basaltic and gabbroic rocks, because of similar REE_N patterns (Campbell et al., 1988; Douville et al., 1999; Klinkhammer et al., 1994; McLennan, 1989). Laboratory experiments have demonstrated that plagioclase dissolution does not control hydrothermal fluid REE patterns (Bach and Irber, 1998; Beermann et al., 2017). Indeed, the REE_N distributions typical of many submarine hydrothermal fluids can be obtained in the absence of plagioclase (Allen and Seyfried, 2005).

In addition to the dissolution of plagioclase and other mineral phases, geochemical modeling and experimental studies have shown that differences in the stability of LREE and HREE aqueous species, differing affinities of each REE in mineral structures, and variations in water-rock ratio control hydrothermal fluid REE concentrations (Allen and Seyfried, 2005; Beermann et al., 2017; Haas et al., 1995; Migdisov et al., 2016; Migdisov and Williams-Jones, 2014; Migdisov et al., 2009). Unlike other REEs that are typically present in the 3+ oxidation state in source rocks and thermal fluids, Eu is largely in the 2+ oxidation state at temperatures above 250 °C (Bau, 1991; Bilal, 1991; Haas et al., 1995; Liu et al., 2017; Sverjensky, 1984). The large difference in ionic radius of 2+ and 3+ Eu ion leads to Eu anomalies in hydrothermal fluids, by affecting the stability of transporting aqueous ligand complexes, and the affinity for inclusion in the structure of secondary minerals formed along flow paths (Allen and Seyfried, 2005; Beermann et al., 2017; Migdisov et al., 2016; Sverjensky, 1984). The transport and fractionation of REE in hydrothermal fluids varies according to a complex interplay of physical factors such and temperature and pressure that influence aqueous speciation and mineral solubility, ligand concentrations, pH, and redox conditions.

Several processes that lead to more variable REE concentrations than typically observed in basalt-hosted submarine hydrothermal fluids have been recognized. Magmatic volatile (e.g. HF, SO_2) fluxes affect relative distributions of REE-F and $REE-SO_4$ complexes that alter availability of REE for incorporation into secondary minerals and modify fluid REE_N patterns (Bach et al., 2003; Craddock and Bach, 2010; Craddock et al., 2010; Sanada et al., 2006). Boiling-induced pH changes in CO_2-rich geothermal fluids have been shown to remove REE from fluids and incorporate them into carbonate well scale in metasedimentary and carbonate hosted geothermal fields (Möller et al., 2008).

To understand controls on the observed REE concentrations in basalt hosted subaerial geothermal systems, we reconstruct fluids to aquifer compositions and model the effects of boiling on the distributions of REE aqueous species and minerals that contain or strongly partition trace REE concentrations. The Haas et al. (1995) thermodynamic dataset for REE aqueous species has been widely used to model REE transport and fractionation in geothermal and hydrothermal fluids (e.g. Bach et al., 2003; Bao et al., 2008; Craddock et al., 2010; Douville et al., 2002; Humphris and Bach, 2005; Lewis et al., 1998; Möller et al., 2008). A limitation of the Haas et al. (1995) dataset is that it was derived from properties measured at room temperature and extrapolated to elevated temperatures. Experimental verification of the Haas et al. (1995) data at hydrothermal temperatures has shown large discrepancies, particularly for REE chloride and fluoride complexes, and the need has been recognized for a revised compilation of experimentally verified thermochemical properties of REE aqueous species for use in geochemical modeling software (c.f. Migdisov et al., 2016).

In this contribution, we investigate geochemical controls on REE fractionation in boiled geothermal fluids from five basalt-hosted and high-temperature (>240 °C) geothermal systems that vary in Cl concentration and pH. Fluid samples were obtained from the Reykjanes, Svartsengi, Hellisheidi, and Nesjavellir geothermal systems located on the Reykjanes peninsula of southwest Iceland, and the Puna geothermal field in Hawaii, USA. The sampled geothermal fluids boiled at pressures between 0.8 and 2.83 MPa, have Cl concentrations (reconstructed for steam loss) that range from less than 1.9 mmol/kg to 502 mmol/kg, and $pH_{(25°C)}$ values that range from 3.94 to 5.77; samples with the highest Cl values correspond to the lowest pH values. For comparison, we provide REE concentration data for fluids from two submarine and sediment-hosted hydrothermal vents from Middle Valley on the Juan de Fuca Ridge that boiled in the subsurface prior to venting at 25 MPa, have Cl concentrations of 432 and 577 mmol/kg, and $pH_{(25°C)}$ values of 5.13 and 5.5. Combined analytical and aqueous geochemical modeling studies of trace elements in the Icelandic geothermal fluids have provided important insights into geothermal processes and the geochemistry of trace elements in geothermal systems (e.g. Kaasalainen and Stefánsson, 2012; Kaasalainen et al., 2015), however REE have not previously been studied in detail for these systems.

2. GEOLOGICAL SETTING

The Reykjanes peninsula of southwest Iceland is a sub-aerial continuation of the submarine Mid-Atlantic Ridge (Fig. 1). The peninsula hosts an en-echelon arrangement of neo-volcanic fissure swarms that are defined by recent eruption sites, fissure swarms and localized seismic activity (Clifton and Kattenhorn, 2006; Jakobsson et al., 1978). The peninsula is underlain by four volcanic systems that have distinct magma supplies and associated geothermal systems (Sæmundsson, 1979). Surface samples from the Reykjanes Peninsula are predominantly tholeiitic basalts (Jakobsson et al., 1978). The subsurface stratigraphy of the Reykjanes peninsula and Hengill volcanic system consist of interlayered subaerial basalt flows, subglacial and submarine pillow basalt and hyaloclastite formations, and an increasing frequency of intrusive rocks with depth (Ármannsson, 2016). Several high-temperature geothermal areas occur along the peninsula, of which Reykjanes, Svartsengi, Hellisheidi, and Nesjavellir are currently utilized for district heating and/or the production of geothermal electricity (Ármannsson, 2016; Arnórsson, 1978, 1995).

Fluids in the Reykjanes geothermal system are composed of seawater chemically modified by boiling and reaction with the basaltic host rock (Arnórsson, 1978; Tomasson and Kristmannsdóttir, 1972). Downhole temperatures of fluids currently produced for geothermal energy in the Reykjanes system range from 270 to 310 °C (Ármannsson, 2016), and temperatures up to 340 °C have been encountered in wells RN-17B and RN-30 (Fowler and Zierenberg, 2016; Fowler et al., 2015; Friðleifsson et al., 2011). More recently, a preliminary minimum temperature of 427 °C was measured in Iceland Deep Drilling Project well IDDP-2 (Friðleifsson et al., 2017; Zierenberg et al., 2017). Secondary minerals in the reservoir of the Reykjanes geothermal system include: albite, actinolite, anhydrite, anorthite, calcite, chalcopyrite, chlorite, epidote, fluorapatite, garnet (grossular/andradite), hornblende, potassium feldspar, pyrite, quartz, and titanite. Progressive alteration mineral sequences with increasing depth and temperature include: mixed-layer smectite–chlorite, chlorite, mixed layer clay chlorite–illite, epidote, actinolite, and amphibole zones (Lonker et al., 1993; Marks et al., 2010; Tomasson and Kristmannsdóttir, 1972).
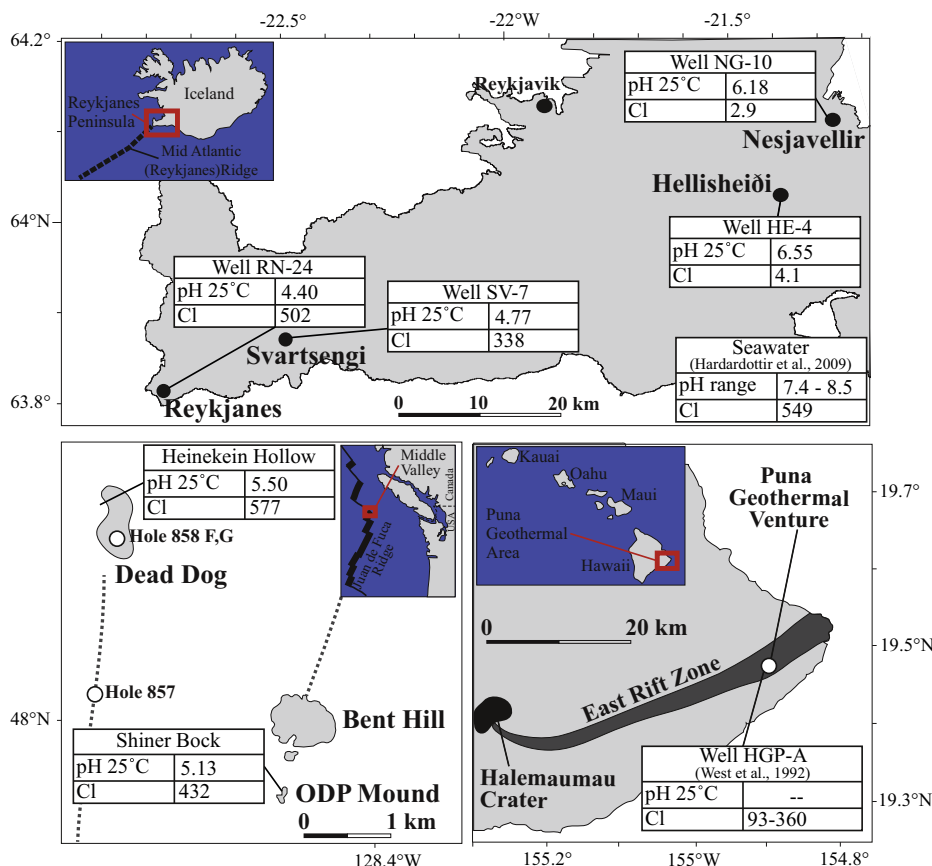
Fig. 1. Sample locations showing representative fluid pH (25 °C) and Cl (mmol/kg) values (corrected for water vapor and gas loss) for each field. Cl and pH values for Icelandic seawater from Hardardóttir et al. (2009) are shown for comparison. Data for geothermal research well HGP-A are from West et al. (1992). Steam and non-condensable gas-corrected pH values are proprietary and are not available for Puna samples. The map of Middle Valley hydrothermal vent sites is modified from Bjerkgård et al. (2000). Middle Valley vent temperatures and Cl concentrations are from Cruse et al. (2008), and pH$_{(25°C)}$ values are from Butterfield et al. (1994), and are corrected to zero magnesium.

The Svartsengi geothermal system is located eastward (inland) of the Reykjanes geothermal system (Fig. 1). Fluids in the Svartsengi geothermal system are derived from a homogenous reservoir, and are a ~2:1 mixture of seawater and meteoric water modified by reaction with the host basalt (Arnórsson, 1978; Ragnarsdóttir et al., 1984). Measured reservoir temperatures in the Svartsengi system are consistently around 240 °C (Ragnarsdóttir et al., 1984). Secondary minerals in the reservoir of the Svartsengi geothermal system include albite, anhydrite, calcite, chalcopyrite, chlorite, epidote, fluorapatite, garnet (grossular and/or andradite), potassium feldspar, pyrite, quartz, and titanite (Lonker et al., 1993).

The Hellisheidi and Nesjavellir geothermal systems are located on the flanks of the Hengill central volcano at the easternmost (inland) extent of the Reykjanes peninsula (Fig. 1). The dilute fluids in the two geothermal systems are meteoric-sourced, and are modified by the influx of magmatic gases and reactions with the host basalt (Ármannsson, 2016). Measured reservoir temperatures range between 270 and 300 °C at Nesjavellir and between 280 and 320 °C in Hellisheidi, although higher temperatures are inferred for the upflow zones (Ármannsson, 2016; Schiffman and Friðleifsson, 1991). Secondary minerals in high-temperature zones of the Hellisheidi and Nesjavellir geothermal system include actinolite, albite, low-Al amphibole, calcite, chlorite, epidote, prehnite, pyrite, quartz, titanite, wairakite, and wollastonite (Ármannsson, 2016; Franzson et al., 1983; Gudmundsson and Arnórsson, 2002; Schiffman and Friðleifsson, 1991).

The Puna geothermal area is located within the East Rift Zone (ERZ) of Kilauea volcano, Hawaii (Fig. 1). The ERZ is a major structural feature that extends from the Kilauea summit caldera approximately 30 km subaerially to the east and continues offshore. Rocks in the subsurface of the lower ERZ have been described using core samples recovered from the 1685 m deep SOH-1 and the 2001 m deep SOH-4 scientific observation core holes (Moore and Truesdell, 1993; Novak and Evans, 1991; Quane et al., 2000). Hole SOH-1 was drilled within a kilometer of the Puna geothermal area, and SOH-4 was drilled ~5 km uprift. Rocks are described as a'a and pahoehoe flows, dikes subparallel to the ERZ, hyaloclastite, breccia, basaltic sand and ash deposits that are increasingly fragmented with increasing depth. Rocks in SOH-1 and SOH-4 are sparsely plagioclase olivine-phyric and are dominated by shield-building tholeiites that are indistinguishable from historical Kilauea lavas to 1685 m depth, the maximum depth of the drill hole (Novak and Evans, 1991; Quane et al., 2000). Hydrothermal alteration in Puna geothermal field is described from samples recovered in the 1962 m deep HGP-A geothermal research well drilled in the Puna geothermal plant lease area (Stone and Fan, 1978). Temperature-dependent alteration mineral sequences in HGP-A are comparable to those observed in Icelandic systems, but the temperature limits between alteration mineral zones occur at higher temperatures in HGP-A. Fluids in the Puna geothermal area are meteoric and seawater that mix in varying proportions on the scale of months (West et al., 1992).

Middle Valley is located at the northern end of the submarine Juan de Fuca Ridge and is an extensional rift filled with turbidites derived from the North American continental margin (Davis et al., 1992). The two main areas of venting at Middle Valley are the Dead Dog Vent Field, and the ODP mound (Fig. 1). The pH$_{(25°C)}$ of fluids in the two main vent locations are estimated at 5.5 and 5.13, respectively (Butterfield et al., 1994). The active hydrothermal mounds and anhydrite chimneys occur along normal faults at 2460 m depth, and vent 184 to 274 °C fluids (Ames et al., 1993; Goodfellow and Franklin, 1993). The subsurface below hydrothermal mounds at Middle Valley consists of hydrothermal feeder zones and massive sulfide mineralization resulting from reactions between hydrothermal fluids and the sediment cover (Zierenberg et al., 1998). Fluids are well below the boiling point at the vent temperature and pressure, however, they are believed to have boiled in the basaltic basement and subsequently reacted with overlying sediments, and the variable input of low salinity vapor produced Cl concentrations lower than seawater in some vents (Butterfield et al., 1994; Cousens et al., 2002; Cruse and Seewald, 2006; Cruse et al., 2008; Goodfellow and Franklin, 1993). Reaction of hydrothermal fluids with sediments and mixing with seawater results in higher pH vent fluids at Middle Valley than typically observed in bare-basalt hosted seafloor hydrothermal systems (Butterfield et al., 1994).

3. METHODS

3.1. Fluid sampling and analysis

Major element and vapor phase analytical results for fluid samples from Reykjanes and Svartsengi geothermal wells were provided by the Iceland Geosurvey (ISOR) on behalf of the field operator (HS Orka hf), from Hellisheidi and Nesjavellir geothermal wells by Orkuveita Reykjavikur (OR), and from the Puna Geothermal field by Ormat technologies, Inc. A schematic of a typical geothermal well is given as Fig. 2. Fluid and vapor samples were collected at the wellheads using a Webré vapor-water separator and analyzed according to the methods described by Arnórsson et al. (2006). Filtered sub-samples for REE analysis were collected in acid-cleaned 120 ml HDPE bottles and acidified using 1 ml of HNO$_3$ (*Trace*SELECT® Ultra from Sigma Aldrich). Fluid samples from the submarine Middle Valley hydrothermal system were collected in July 2000 (Cruse et al., 2008), and sub-samples for REE analysis were provided by Jeffrey Seewald (Woods Hole Oceanographic Institution). Mg-corrected major element, gas, and trace metal data for the Middle Valley samples have been reported previously (Cruse et al., 2008).

Fluid samples for REE analysis were prepared using a modified (offline) version of the Zhu et al. (2010) pre-concentration method. A commercially available brand of syringe driven chelating column (SDCC; InertSEP ME-1 packed with 280 mg of iminodiacetate chelating resin; GL Sciences, Torrence, CA) was used to pre-concentrate samples. Reagents included ultrapure grade (*Trace*SELECT® Ultra) ammonium hydroxide and acetic acid (Sigma
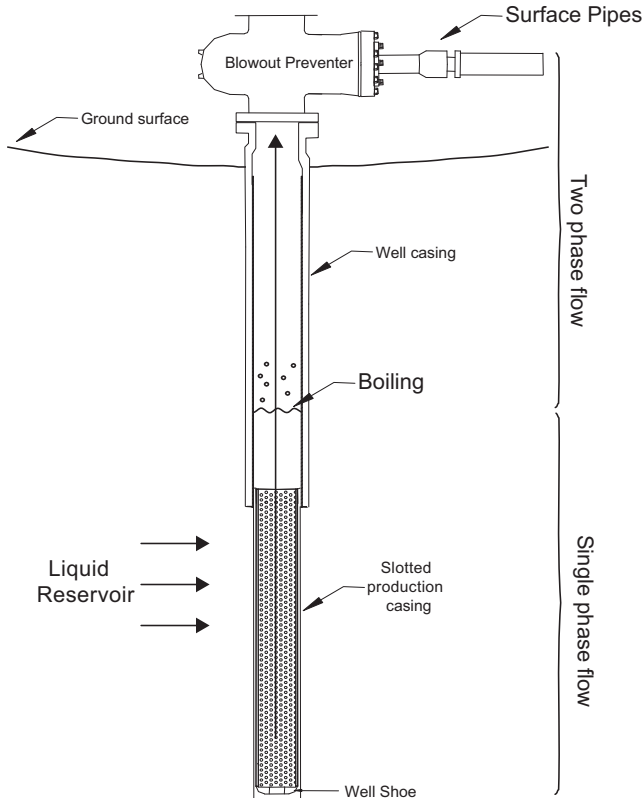
Fig. 2. Schematic of a typical geothermal well.

Aldrich, Inc.), double distilled sub boiling nitric acid (2 M and 3 M), and Milli-Q water (18.3 MΩ). Ammonium acetate (1.8 M) was prepared from the reagents and used to adjust 20 ml aliquots of samples to pH 5, verified using a non-contact pH meter (Horriba B-213). Reagent and sample flow rates into the SDCC were controlled using an automated syringe pump.

The SDCC's were soaked overnight in Milli-Q water prior to use. Reagents and samples were introduced to the SDCC in the following order: (1) SDCC cleaning with 5 ml of HNO_3 (3 M) at 5 ml min^{-1}; (2) SDCC conditioning with 5 ml ammonium acetate (1 M) (NH$_4$Ac) at 5 ml min^{-1} followed by 2.5 ml Milli-Q at 5 ml min^{-1}; (3) loading 20 ml of sample to the SDCC at 5 ml min^{-1}, (4) sample elution using 2.5 ml HNO_3 (2 M) at 1 ml min^{-1}. An internal standard (In-Bi-Re) was added to each sample to correct for sample matrix effects and instrument drift, and a Tm spike was added to each sample to verify REE recovery. The overall preconcentration factor of analyzed samples was approximately 8.

Samples were analyzed at UC Davis using a Thermo Scientific Element XR magnetic sector ICP-MS working in low-resolution mode (m/Δm = 300); operating parameters are provided as supplemental file A1. Oxide production was tuned to less than 5% using a uranium solution and monitoring the 238/254 mass ratio. Oxide production was periodically (~every 10 samples) monitored during the run by measuring a single element cerium standard (10 ppb) and monitoring the 140/156 mass ratio. Oxide

interferences were corrected for using the method of (Aries et al., 2000), however owing to low oxide production the correction was negligible. Analytical precision was verified by analyzing sample duplicates from each geothermal field, and accuracy was verified by analyzing multiple aliquots of CASS-4 and NASS-6 seawater reference standards that were processed independently through the entire preconcentration and analytical method. The method detection limit (MDL) is defined as 6 times the standard deviation of 16 replicate measurements of the NASS-6 seawater standard in pmol/kg was: Y (49), La (20), Ce (8.3), Pr (3.3), Nd (16), Sm (3.6), Eu (0.9), Gd (2.3), Tb (1.2), Dy (5.6), Ho (1.7), Er (5.1), Yb (6.1), and Lu (0.9).

3.2. Apatite and pipe scale analysis

Well scale samples were collected from surface pipes connected to well RN-9 in the Reykjanes geothermal system. Well RN-9 was drilled from the same well pad as wells RN-21 and RN-24 and about 300 m northeast of well RN-12. The fluid composition (Cl = 522 to 544 mmol/kg) and measured temperature (~290 °C) is comparable to the surrounding wells (Hardardóttir, 2002). Samples of precipitates from surface pipes exiting well RN-9 were analyzed for REE at Actlabs, Ontario, Canada.

The composition of apatite present in the drill core samples was characterized to provide a modeling constraint on the pre-boiled phosphorous concentration in geothermal fluids. Drill core samples were obtained from Iceland Deep

Drilling Project (IDDP) core RN-30, which was recovered from the Reykjanes geothermal system (Fowler and Zierenberg, 2016). Back scattered electron (BSE) imaging and electron microprobe (EMP) analysis of apatite were performed using a Cameca SX-100 EMP the University of California Davis, Department of Earth and Planetary Sciences (UC Davis). EMP operating parameters for fluorapatite analyses were an accelerating voltage of 15 kV, a beam current of 10 nA, and a beam diameter of 1 μm. Peak counting times were 10 s (Si and Nd), 20 s (La, Ce, Sm and P), 30 s (Ca, Y, and Cl), and 60 s (F). The following calibration standards were used: Wilberforce apatite (Ca, P and F), scapolite (Cl), SiO_2 (Si), a synthetic YPO_4 crystal (Y), a synthetic $LaPO_4$ crystal (La), a synthetic $CePO_4$ crystal (Ce), a synthetic $SmPO_4$ crystal (Sm), and a synthetic $NdPO_4$ crystal (Nd). Cation totals were calculated based on $26O + F + Cl$ atoms and OH was calculated by difference.

3.3. Geochemical modeling

Chemical equilibrium calculations were completed using the programs SOLVEQ-XPT (Reed et al., 2016a) and CHIM-XPT (Reed et al., 2016b). SOLVEQ-XPT computes homogenous equilibrium (the distribution of aqueous chemical species) at given pressure and temperature conditions. CHIM-XPT computes heterogeneous chemical equilibrium that allows for perturbations in composition, pressure and temperature to model complex processes including boiling. SOLVEQ-XPT and CHIM-XPT compute equilibria at any specified pressure and temperature up to 500 MPa and 600 °C, except for the steam phase region and where water density is less than 0.35 g/cc at higher T and P beyond the critical point of water. Calculations are not constrained to the liquid-vapor saturation state of H_2O. SOLTHERM, the thermodynamic database read by SOLVEQ-XPT and CHIM-XPT, is revised to include the most current thermodynamic data for REE aqueous species and REE-bearing minerals (Palandri and Reed, 2016). These data include experimentally derived data for aqueous REE fluoride, chloride, and sulfate complexes (Migdisov and Williams-Jones, 2008; Migdisov et al., 2009), along with data for REE-phosphate minerals compiled by (Migdisov et al., 2016). Experimentally determined data for REE carbonate, phosphate, and hydroxide complexes at elevated temperatures are currently unavailable, therefore, the theoretical predictions of Haas et al. (1995) for these aqueous REE species is used. With the exception of aqueous fluoride complexes (Haas et al., 1995), thermodynamic data for aqueous Eu^{2+} species are not available. To overcome this limitation, log K values for aqueous Eu^{2+} species ($EuCO_{3(aq)}$, $EuHCO_3^+$, $EuCl^+$, EuF^+, and $EuOH^+$) were based on the average of log K values for Sr^{2+} and Ca^{2+} aqueous species, following the approach of (Liu et al., 2017). REE species and minerals included in SOLTHERM are listed on Table 1. The revised database is freely available for download from http://pages.uoregon.edu/palandri/. Redox in the models was constrained using measured sulfide-sulfate concentrations (Reed, 1982), which approach equilibrium concentrations

in saline Icelandic geothermal systems (Stefánsson and Arnórsson, 2002).

3.4. Reconstructing the pre-boiled reservoir fluid

High temperature Icelandic geothermal wells discharge a mixture of liquid and vapor during sampling, due to a decrease in pressure from reservoir conditions to the pressure controlled at the sampling orifice. Many chemical species are concentrated in the liquid phase and volatile species and non-condensable gases are fractionated into the vapor phase. Samples of both the liquid and vapor phase and an estimate of the steam/liquid fraction are required to mathematically reconstruct the composition of the reservoir fluid. The value used for the steam fraction influences calculated pH and redox conditions, critical parameters for calculating the distribution of aqueous species and solubility of minerals (Reed, 1982). In cases where the reservoir fluid approximates a single liquid phase and adiabatic boiling assumptions are valid a simple mass balance can be used to calculate the steam fraction (Henley, 1984):

$$X_{steam} = \left(H_{reservoir} - H_{liquid}\right) / \left(H_{vapor} - H_{liquid}\right) \qquad (1)$$

where X_{steam} is the steam fraction, $H_{reservoir}$ is the enthalpy at the liquid-vapor saturation point equivalent to the measured reservoir temperature, and H_{vapor} and H_{liquid} are the enthalpies of water vapor and liquid at saturation taken from steam tables (e.g. Wagner and Kretschmar, 2008) at the sampling pressure. The concentration of a component in the reservoir ($M_{reservoir}$) can then be recalculated from its concentration in the liquid (M_L) or in the steam phase (M_V) collected at the well head, equivalent to:

$$M_{reservoir} = (1 - X_{steam}) \times M_L \qquad (2)$$

And the concentration of a component in the steam phase is equivalent to:

$$M_{reservoir} = X_{steam} \times M_V \qquad (3)$$

Gas and liquid-phase analytical results for boiled geothermal fluids (Table 2) are then mathematically recombined to calculate the pH and dissolved constituent concentrations in pre-boiled fluids according to the method of Reed and Spycher (1984), using the computer program GEOCAL-XPT (Reed et al., 2016a). Data for major elements, non-condensable gases, or downhole temperature were not available from the Puna geothermal field for proprietary reasons, but sampling pressures were provided. For this reason, we report only steam-loss corrected REE concentration data for Puna wells. The estimated maximum downhole temperature for Puna (350 °C) is based on results from the HGPA research well and likely overestimates the steam fraction, thus, underestimates dissolved REE concentrations in downhole fluids.

The plausibility of reconstructed fluids was evaluated by comparing secondary minerals observed in drill samples to secondary minerals calculated to be at saturation in the reconstructed fluids. This was accomplished by constructing Q/K mineral saturation diagrams (Reed and Spycher, 1984) using SOLVEQ-XPT. The estimated reservoir temperature determined from Q/K diagrams was then used to

Table 1
Aqueous REE species and REE-bearing mineral thermodynamic data utilized in speciation and boiling models.

Notes	Aqueous REE species[*]	Formula	Source
	Simple hydrated ions	$REE{++}$; $REE{+++}$; $REE{++++}$	Sverjensky (1984), Shock and Helgeson (1988), Shock et al. (1997)
1	Hydroxides	$REEOH\ ++$; $REE(OH)_2+$; $REE(OH)_{3(aq)}$; $REE(OH)_4-$	Haas et al. (1995)
1	Carbonates	$REECO_3+$; $REEHCO_3++$	Haas et al. (1995)
1	Nitrate	$REENO_3++$	Haas et al. (1995)
1	Phosphate	$REEH_2PO_4++$	Haas et al. (1995)
2	Sulfates	$REESO_4+$; $REE(SO4)_2-$	Migdisov and Williams-Jones (2008)
3	Chlorides	$REECl++$; $REECl_2+$	Migdisov et al. (2009)
3	Fluoride	$REEF++$	Migdisov et al. (2009)
4	Eu(II) species	$EuCO_{3(aq)}$, $EuHCO_3+$, $EuCl+$, $EuF+$, and $EuOH+$	

Notes	Solids	Formula	Source
5	REE Metal	REE	Robie et al. (1978), Robie and Hemingway (1995)
	REE hydroxide	$REE(OH)_3$ (s)	Diakonov et al. (1998a), Diakonov et al. (1998b), Diakonov et al. (1998c)
5,6,7	REE oxide	$REE^{2+}O_2$	Robie et al. (1978), Robie and Hemingway (1995)
7	di-REE trioxide	$REE_2^{3+}O_3$	Robie et al. (1978)
	Allanite	$CaCeFeAl_2(SiO_4)_3OH$	Spear (2010)
	Dissakisite-La	$CaLaMgAl_2(SiO_4)_3OH$	Janots et al. (2007)
	Monazite	Y, La, Ce, Pr, Nd, Sm, Eu, and Gd $-PO_4$	Migdisov et al. (2016)
	Xenotime-	Tb, Dy, Er, Yb, Lu, and Y, $-PO_4$	Migdisov et al. (2016)
	Apatite-F, –OH, –Cl	$Ca_5(PO_4)_3(OH, F, Cl)$	Zhu and Sverjensky (1991)

Notes:
1. Extrapolated to elevated temperatures from association constants measured at 25 °C.
2. Experimentally determined association constants at elevated temperatures interpolated to Eu, Gd, Tb, Dy and Ho; extrapolated to La, Ce, Pr, Tm, Yb, Lu.
3. Experimentally determined association constants at elevated temperatures.
4. Average of Log K values for corresponding Sr(II) and Ca(II) species.
5. Data for cerium and CeO_2 from Robie and Hemingway (1995); others from Robie et al. (1978).
6. PrO suppressed due to anomalously large Q/K.
7. TbO and Tb_2O_3 absent due to lack of molar volume data.
8. Does not contain REE in formula or models, but strongly partitions REE (e.g. Fleet and Pan, 1995a,b).

constrain concentrations of components that were not analyzed in fluid samples or components that had suspect concentrations owing to sequestration in well scale minerals. These uncertain concentrations were constrained by forcing equilibrium with minerals observed in drill cuttings and well scale according to the method of Pang and Reed (1998). Fe was constrained using pyrite, Cu with chalcopyrite, Pb with galena, Zn with sphalerite, and P with fluorapatite.

3.5. Isenthalpic boiling models

To further investigate the controls of aqueous speciation and phosphate mineral precipitation on REE concentrations in the Icelandic geothermal fluids, isenthalpic boiling models were completed using CHIM-XPT. Details of the approach are provided by Spycher and Reed (1989). Two boiling models were completed for the samples from wells RN-24 at Reykjanes, SV-7 at Svartsengi, and HE-4 at Hellisheidi. The Puna geothermal system was not investigated further because proprietary fluid major element, gas, and well scale composition data required to model boiling were

not available. The first boiling model for each well was designed to accommodate higher REE in deep fluids, and to investigate the saturation state of REE-bearing solids and changes in REE speciation as boiling progressed. In these models the average value for REE in submarine hydrothermal fluids for which yttrium data are available was used (i.e. Bao et al., 2008; Douville et al., 1999; Douville et al., 2002). The second boiling model was completed with no REE present in fluids (REE-free models) to identify the formation of solid phases that partition trace concentrations of REE that might be prevented from forming in the models using higher REE-concentrations.

3.6. Zero magnesium correction

The pressure resulting from 2460 m of overlying cold seawater prevents Middle Valley hydrothermal fluids from boiling at the vent, so corrections for vapor loss were not necessary. During sampling of seafloor hydrothermal fluids, dead space in titanium sampling apparatus is filled with seawater, and ambient seawater can be entrained during collection. The composition of the unmixed hydrothermal

Table 2
Raw analytical results for major elements, gases, and REE in geothermal fluids from Iceland and Hawaii, and submarine hydrothermal fluids from Middle Valley.

Well		RN-12	RN-12DUP	RN-18	RN-21	RN-24	SV-07	SV-11	SV-11DUP	NG-7	NG-7DUP	NG-10	HE-4	HE-5	HE-11	KS-5	KS-6W	KS-9W	KS-14E	KS-16N	KS-16NDUP	Heineken Hollow	Heineken Hollow DUP	Heineken Hollow	Shiner Bock
Field		Reykjanes	Reykjanes	Reykjanes	Reykjanes	Reykjanes	Svartsengi	Svartsengi	Svartsengi	Nesjavellir	Nesjavellir	Nesjavellir	Hellisheiði	Hellisheiði	Hellisheiði	Puna	Puna	Puna	Puna	Puna	Puna	Dead Dog	Dead Dog	Dead Dog	ODP Mound
Date		17–02–2015	17–02–2015	23–10–2014	17–02–2015	23–10–2014	05–11–2014	05–11–2014	05–11–2014	19–11–2014	19–11–2014	19–11–2014	13–08–2014	13–11–2014	22–09–2014	09–11–2016	09–11–2016	11–11–2016	11–11–2016	07–11–2016	10–11–2016	22–06–1905	22–06–1905	22–06–1905	22–06–1905
Sample		20,150,037	20,150,037	20,140,369	20,150,038	20,140,370	20,140,386	20,140,387	20,140,387	2014–5400	2014–5400	2014–5399	2014–5270	2014–5394	2014–5326	42,683	42,683	42,685	42,681	42,684	42,684	M3596-12C	M3596-12C	M3597-15	M3595-12
Sampling T	°C	–	–	–	–	–	–	–	–	–	–	–	–	–	–	–	–	–	–	–	–	187	187	187	272
Sampling P	bar-g	28.3	28.3	23.2	26.2	24.0	14.6	17.3	17.3	13.5	13.5	13.5	8.5	8	8.2	17.4	17.4	16.5	17.5	18.1	18.1	~250	~250	~250	~250
Wellhead P	bar-g	–	–	–	–	–	–	–	–	21	21	19	13	16	14	–	–	–	–	–	–	–	–	–	–
Discharge Enthalpy	kJ/kg	–	–	–	–	–	–	–	–	1236	1236	1215	1056	1232	2117	–	–	–	–	–	–	–	–	–	–
Analytical methods		a,d	d	a,d	a,d	a,d	a,d	a,d	d	b,d	d	b,d	b,d	b,d	b,d	d	d	d	d	d	d	c,d	c,d	c,d	c,d
Liquid phase																									
pH/Temp.	pH/°C	5.60/21.5	–	6.05/21.2	5.84/21.6	5.81/21.5	6.07/20.9	5.9/21.3	–	8.59/22.1	–	8.79/22.4	9.28/21.6	9.15/19.1	8.70/18.0	6.31/25.0	5.28/25.0	5.7/25.0	5.56/25.0	5.46/25.0	5.46/25.0	5.50	–	5.50	5.13
Cl	mmol/kg	611	–	581	587	604	376	378	–	2.9	–	3.6	4.9	2.6	4.3	–	–	–	–	–	–	581	–	554	435
F	mmol/kg	0.014	–	0.012	0.012	0.012	0.011	0.010	–	–	–	0.071	0.031	0.093	0.057	–	–	–	–	–	–	–	–	–	–
SO4	mmol/kg	0.08	–	0.12	0.10	0.13	0.26	0.27	–	0.14	–	0.18	–	0.18	0.10	–	–	–	–	–	–	2.04	–	14.6	2.11
SiO2	mmol/kg	13.2	–	12.0	11.2	12.3	7.9	8.3	–	11.39	–	12.51	10.04	11.62	11.58	–	–	–	–	–	–	–	–	–	–
B	mmol/kg	0.79	–	0.77	0.76	0.78	0.62	0.68	–	–	–	–	–	–	–	–	–	–	–	–	–	–	–	–	–
Na	mmol/kg	475	–	450	459	467	294	294	–	7.49	–	7.77	8.72	7.51	7.60	–	–	–	–	–	–	416	–	422	361
K	mmol/kg	39.9	–	37.9	39.1	39.4	25.3	25.3	–	0.76	–	0.84	0.77	0.79	0.82	–	–	–	–	–	–	19.4	–	15.0	14.2
Ca	mmol/kg	47.2	–	39.9	41.7	42.4	25.5	25.7	–	0.011	–	0.009	0.018	0.012	0.010	–	–	–	–	–	–	72.5	–	45.7	36.2
Mg	mmol/kg	0.040	–	0.018	0.027	0.014	0.020	–	–	<0.002	–	<0.002	<0.003	<0.002	<0.003	–	–	–	–	–	–	3.13	–	27.9	3.10
Al	µmol/kg	2.3	–	3.3	3.8	3.3	2.8	2.5	–	66	–	74	57	71	73	–	–	–	–	–	–	–	–	–	–
Ba	µmol/kg	70.2	–	57.6	65.2	65.9	12.0	12.7	–	–	–	–	–	–	–	–	–	–	–	–	–	–	–	–	–
Cu	µmol/kg	<0.0079	–	0.02	<0.0079	<0.0079	<0.0079	<0.0079	–	–	–	–	–	–	–	–	–	–	–	–	–	0.3	–	0.9	2.3
Fe	µmol/kg	4.3	–	1.0	3.0	2.0	1.0	1.1	–	<0.7	–	<0.7	<0.9	<0.7	<0.9	–	–	–	–	–	–	22	–	5.1	35
Sr	µmol/kg	114	–	100	108	109	82	83	–	–	–	–	–	–	–	–	–	–	–	–	–	245	–	176	152
Zn	µmol/kg	<0.31	–	0.09	<0.31	<0.08	0.28	<0.06	–	–	–	–	–	–	–	–	–	–	–	–	–	1.1	–	0.25	1.6
CO2	mmol/kg	1.16	–	0.9	0.5	0.8	1.1	0.8	–	1.2	–	0.6	0.7	1.7	0.9	–	–	–	–	–	–	–	–	–	–
H2S	mmol/kg	0.12	–	0.03	0.05	0.04	0.02	0.06	–	2.4	–	1.8	1.5	0.8	1.6	–	–	–	–	–	–	–	–	–	–
NH3	mmol/kg	0.073	–	0.06	0.07	0.07	0.05	0.05	–	–	–	–	–	–	–	–	–	–	–	–	–	–	–	–	–
Y	pmol/kg	<49	17	<49	<49	<49	<49	<49	14	<49	<49	<49	<49	<49	<49	<49	55	<49	28	28	26	1729	1631	612	136
La	pmol/kg	276	272	236	126	120	78	84	84	40	39	39	40	42	43	<20	34	17	25	42	45	2536	2385	1570	786
Ce	pmol/kg	7.6	8.1	15	19	11	10	7.6	7.9	4.7	4.7	4.7	8.1	13	9	8.4	15	13	13	23	26	3350	3136	1822	1196
Pr	pmol/kg	<3.3	<3.3	1.5	1.5	<3.3	<3.3	<3.3	<3.3	<3.3	<3.3	<3.3	<3.3	<3.3	<3.3	<3.3	<3.3	<3.3	<3.3	2.6	2.6	350	326	159	120
Nd	pmol/kg	<16	<16	<16	<16	<16	<16	<16	<16	<16	<16	<16	<16	<16	<16	<16	12	<16	<16	10	9.4	1296	1214	537	346
Sm	pmol/kg	1.6	1.7	2.3	2.2	1.8	<3.6	<3.6	<3.6	<3.6	<3.6	<3.6	<3.6	<3.6	<3.6	5.6	<3.6	<3.6	2.5	2.5	2.3	223	208	75	17
Eu	pmol/kg	30	31	32	43	38	8.7	10	10	<0.9	<0.9	<0.9	0.5	<0.9	<0.9	30	240	53	100	96	90	4336	4025	690	121
Gd	pmol/kg	<0.35	<0.35	<0.35	<0.35	<0.35	<0.35	<0.35	<0.35	<0.35	<0.35	<0.35	<0.35	<0.35	<0.35	<0.35	<0.35	<0.35	<0.35	<0.35	<0.35	42.2	38.3	16.6	6.9
Tb	pmol/kg	<1.2	<1.2	0.2	0.3	0.2	<1.2	<1.2	<1.2	<1.2	<1.2	<1.2	<1.2	<1.2	<1.2	<1.2	<1.2	<1.2	<1.2	<1.2	<1.2	29	28	7.8	2.6
Dy	pmol/kg	<0.94	<0.94	<0.94	<0.94	<0.94	<0.94	<0.94	<0.94	<0.94	<0.94	<0.94	<0.94	<0.94	<0.94	<0.94	<0.94	<0.94	<0.94	<0.94	<0.94	25.6	24.1	5.6	1.7
Ho	pmol/kg	<0.27	<0.27	<0.27	<0.27	<0.27	<0.27	<0.27	<0.27	<0.27	<0.27	<0.27	<0.27	<0.27	<0.27	<0.27	<0.27	<0.27	<0.27	<0.27	<0.27	5.1	4.8	1.1	0.4
Er	pmol/kg	<0.85	<0.85	<0.85	<0.85	<0.85	<0.85	<0.85	<0.85	<0.85	<0.85	<0.85	<0.85	<0.85	<0.85	<0.85	<0.85	<0.85	<0.85	<0.85	<0.85	14.5	13.5	2.7	1.0
Tm	pmol/kg	–	–	–	–	–	–	–	–	–	–	–	–	–	–	–	–	–	–	–	–	–	–	–	–
Yb	pmol/kg	4.0	3.8	3.5	5.5	3.5	0.8	0.8	0.6	<6.1	<6.1	<6.1	<6.1	<6.1	<6.1	<6.1	<6.1	<6.1	<6.1	<6.1	<6.1	72	73	12	6.1
Lu	pmol/kg	1.4	1.5	1.4	1.4	0.9	0.3	0.3	0.3	<0.9	<0.9	<0.9	<0.9	<0.9	<0.9	<0.9	1.0	<0.9	0.5	<0.9	<0.9	12	13	2.6	1.5
Tm Spike Recovery	(%)	94%	92%	98%	83%	95%	92%	91%	91%	96%	94%	98%	98%	92%	92%	95%	100%	100%	107%	101%	–	97%	93%	90%	91%
Vapor phase																									
Gas/Condensate	L/kg	–	–	–	–	–	–	–	–	1.746	–	0.286	0.117	0.165	0.506	–	–	–	–	–	–	–	–	–	–
Temp.	°C	–	–	–	–	–	–	–	–	–	–	–	–	–	–	–	–	–	–	–	–	–	–	–	–
CO2	mmol/kg	283	–	153	110	184	141	248	–	93	–	42	35	81	91	–	–	–	–	–	–	–	–	–	–
H2S	mmol/kg	9.7	–	5.3	5.0	5.6	4.7	7.9	–	26.9	–	18.1	10.2	6.7	20.8	–	–	–	–	–	–	–	–	–	–
H2	mmol/kg	0.31	–	0.97	1.13	0.28	1.40	2.56	–	–	–	–	–	–	–	–	–	–	–	–	–	–	–	–	–
N2	mmol/kg	2.76	–	2.50	2.16	2.56	1.66	2.14	–	–	–	–	–	–	–	–	–	–	–	–	–	–	–	–	–
O2	mmol/kg	0.69	–	<0.001	9.08	<0.001	<0.001	<0.001	–	–	–	–	–	–	–	–	–	–	–	–	–	–	–	–	–
Ar	mmol/kg	0.058	–	0.051	0.047	0.052	0.034	0.044	–	–	–	–	–	–	–	–	–	–	–	–	–	–	–	–	–
CH4	mmol/kg	0.072	–	0.042	0.024	0.058	0.033	0.053	–	–	–	–	–	–	–	–	–	–	–	–	–	–	–	–	–
NH3	mmol/kg	0.21	–	0.21	0.22	0.18	0.18	–	–	–	–	–	–	–	–	–	–	–	–	–	–	–	–	–	–
Na	mmol/kg	0.018	–	0.009	0.016	0.011	0.010	0.008	–	–	–	–	–	–	–	–	–	–	–	–	–	–	–	–	–
B	mmol/kg	0.024	–	0.026	0.027	0.055	0.022	0.035	–	–	–	–	–	–	–	–	–	–	–	–	–	–	–	–	–
H2	% Vol.	–	–	–	–	–	–	–	–	86.48	–	23.31	34.24	7.31	90.91	–	–	–	–	–	–	–	–	–	–
N2	% Vol.	–	–	–	–	–	–	–	–	15.1	–	65.4	42.5	83.3	5.0	–	–	–	–	–	–	–	–	–	–
O2	% Vol.	–	–	–	–	–	–	–	–	0.00	–	0.45	0.00	0.00	0.00	–	–	–	–	–	–	–	–	–	–
CH4	% Vol.	–	–	–	–	–	–	–	–	3.11	–	11.76	18.54	6.24	1.79	–	–	–	–	–	–	–	–	–	–

– Not measured.

< Less than specified method detection limit.

DUP Sample duplicate for REE + Y independently processed through entire analtyical method.

a. Analyses performed by Icelandic Geosurvey (ISOR); anions by IC, major cations by AAS, trace cations by ICP, CO_2 and H_2S by titration, NH_3, B and SiO_2 by spectrophotometry and the non-acidic gases by GC.

b. Analyses performed by Orkuveita Reykjavikur. All samples were analzyed using ion chromatography.

c. Major element data from Cruse et al. (2008) and pH from Butterfield et al. (1994).

d. REE + Y analysed by preconcentration and ICP-MS (This study).

Method Detection Limit (MDL) for REE analyses = 6 * standard deviation of 16 replicate measurements of NASS-6 seawater standard. REE concentrations below the MDL but greater than 3 * SD of 16 replicate measurements of NASS-6 seawater standard are given in italics.

end-member fluid is determined using a zero Mg correction that requires knowledge of analyte concentrations in an ambient seawater sample (Von Damm et al., 1985). No ambient seawater REE analyses or samples were available from Middle Valley. Instead, an ambient seawater sample collected near Baby Bare warm spring $\sim$100 km from Middle Valley (Wheat et al., 2002) was used for the zero-Mg correction. Zero-Mg corrected Middle Valley fluids were then modelled in the liquid phase region of water at a pressure of 246 bar and the measured temperatures at each specific vent. Details of the zero Mg calculation are provided as supplemental file A2.

4. RESULTS

4.1. Fluid analytical results

Raw analytical results for major elements, trace elements, and dissolved gases in the Icelandic geothermal fluids are provided in Table 2, and detection limits are provided by Arnórsson et al. (2006). Parameters used for the steam loss correction are given in Table 3. Results for REE in the CASS-4 and NASS-6 seawater standards agree with published values (Fig. 3). Tm spike recoveries in the standards ranged from 96 to 108%. REE in duplicate samples were within 5% of the primary sample concentration, except Gd (5.2%) and Lu (5.6%) in the Heineken Hollow sample from Middle Valley, and Ce (7.6%) in Puna sample KS-9 W. Tm spike recoveries in the samples ranged from 90 to 107%. Oxide production remained steady during analytical runs based on the 140/156 mass ratio periodically measured on a single element cerium solution. Tabulated results for standards, duplicate samples, and spike recoveries for REE measurements are provided in supplemental file A3.

Results for REE in basalt-hosted geothermal fluids (corrected for steam loss) and Middle Valley hydrothermal fluids (corrected to Mg = 0) are presented in Table 4 and Fig. 4. Overall, REE concentrations in basalt-hosted geothermal fluids are lower than any value previously reported for basalt-hosted submarine hydrothermal vent fluids (Fig. 4A–C). Middle Valley vent fluid REE concentrations and REE_N patterns are typical of the range reported for submarine hydrothermal vent fluids.

Reykjanes, Svartsengi and Puna geothermal fluid samples are characterized by elevated chondrite normalized La and Eu concentrations, measurable Ce, and all other REE are absent at levels above respective MDL's except for Lu in the Reykjanes samples for which the MDL was particularly low (0.2 pmol/kg) (Fig. 4A and B). REE are absent in fluids from Hellisheidi and Nesjavellir at levels above the MDL except for La (and Ce in well HE-5), a finding at odds with much higher REE concentrations reported by Aggarwal et al. (1996) for fluids from Nesjavellir well NJ-11 (Fig. 4C). The value of 0.013×10^{-9} moles/kg for Ce in the liquid fraction (no steam loss correction) for well HE-5 measured in this study is in agreement with Ce concentrations ranging from $<0.007 \times 10^{-9}$ to 0.010×10^{-9} moles/kg reported for the liquid fraction sampled from several Hellisheidi wells by Alfredsson et al. (2013).

West et al. (1992) reported REE concentrations for fluids from the HGP-A geothermal research well of 29–29833 pmol/kg for La, 43–1385 pmol/kg for Ce, and 66–3159 pmol/kg for Eu, noting that REE in HGP-A fluids are mostly close to pmol/kg-level detection limits at the lower end of this range, and are orders of magnitude lower than for typical submarine hydrothermal fluids. Our results for REE in fluids from Puna wells (not corrected for steam loss) are consistent with the lower limit of REE values reported for the HGP-A geothermal research well (i.e. < 20–25 pmol/kg for La, <8.3–14 pmol/kg for Ce, and 18–144 pmol/kg for Eu).

4.2. Analytical results for well RN-9 surface pipe scale samples

The mineralogy of the RN-9 surface pipe scale samples has been described in detail previously (Hardardóttir, 2002; Hardardóttir et al., 2010). Briefly, the scale samples are predominantly amorphous Fe-rich silica with sphalerite, chalcopyrite, trace galena, and occasional pyrrhotite, bornite and covellite. The composition of the samples ranges from 45.21 to 85.45 weight % SiO_2 with Cu, Zn and Pb in the parts per thousand range, and detectable REE and phosphorous (Table 5). Chondrite normalized REE scale concentrations are fractionated relative to unaltered basalts, with higher LREE relative to HREE concentrations (Fig. 5). Absolute well scale REE concentrations are lower than unaltered tholeiite (i.e. Fowler and Zierenberg, 2016), but several orders of magnitude higher than for Reykjanes fluids.

4.3. Apatite EMP results

Fluorapatite (fluorine apatite endmember: $Ca_5(PO_4)_3F$) was identified in the altered groundmass of basaltic intrusions from drill core RN-30 recovered by the Iceland Deep Drilling Project from the Reykjanes geothermal system. Reykjanes fluorapatite is present in albitized vugs in a sample from 2514.33 m and chloritized igneous mesostasis interstitial to primary igneous phases in samples from 2512.53 m, 2516.06 m, and 2530.24 m. Fluorapatite in the sample from 2514.33 m forms acicular hexagonal needles up to $\sim$ 400 μm long by 10 μm wide (supplemental file A4). The size of fluorapatite needles in the sample from 2514.33 m are amenable to EMP analysis, but are $\ll$10 μm in other depth intervals and too small for EMP analysis. Fluorapatite in vugs is encased in secondary albite/anorthite intergrowths in the 2514.33 m sample, and it bisects primary igneous clinopyroxene grains indicating it is a secondary mineral (supplemental file A4 Figures C–E). The clinopyroxene exhibits a hackly and diffuse grain edges that are flooded by chlorite (supplemental file A4 Figures A–F), indicating dissolution along grain boundaries. Major secondary phases associated with fluorapatite commonly include chlorite, albite, and quartz. Chlorite replaces albite as the dominant associated major phase in other depth intervals. Minor secondary phases associated with fluorapatite commonly include chalcopyrite and titanite

Table 3
Parameters used to calculate steam loss from boiling of geothermal fluid samples included in the present study.

Well	Geothermal field	Sample date	[1]Reservoir temp. (°C)	[2]Sampling pressure (bar)	[3]Reservoir enthalpy (kJ/kg)	[4]Well head liquid enthalpy (kJ/kg)	[4]Well head vapor enthalpy (kJ/kg)	[5]Steam fraction
RN-12	Reykjanes	17–02–2015	296	29.3	1322.54	995.05	2803.11	0.18
RN-18	Reykjanes	23–10–2014	285	24.2	1263.03	941.626	2800.92	0.17
RN-21	Reykjanes	17–02–2015	285	27.2	1263.03	971.74	2802.45	0.16
RN-24	Reykjanes	23–10–2014	285	25.0	1263.03	951.952	2801.54	0.17
SV-07	Svartsengi	05–11–2014	238	15.6	1028.00	837.516	2789.98	0.10
SV-11	Svartsengi	05–11–2014	240	18.3	1037.52	878.316	2795.28	0.08
KS-5f	Puna	09–11–2016	350	18.4	1670.86	890.788	2796.65	0.41
KS-6Wf	Puna	09–11–2016	350	18.4	1670.86	890.788	2796.65	0.41
KS-9Wf	Puna	11–11–2016	350	17.5	1670.86	878.316	2795.28	0.41
KS-14Ef	Puna	07–11–2016	350	18.5	1670.86	890.788	2796.65	0.41
KS-16Nf	Puna	10–11–2016	350	19.1	1670.86	896.844	2797.26	0.41
NG-10	Nesjavellir	19–11–2014	290	14.5	1215	822.552	2787.73	0.20
NG-7	Nesjavellir	19–11–2014	275	14.5	1236	822.552	2787.73	0.21
HE-4	Hellisheiði	13–08–2014	260	9.5	1056	732.113	2770.76	0.16
HE-5	Hellisheiði	13–11–2014	262	9	1232	721.018	2768.30	0.25
HE-11	Hellisheiði	22–09–2014	275	9.2	2117	721.018	2768.30	0.68

1. Reservoir temperatures from: Fridriksson and Giroud (2008); Bjornsson et al. (1998); Steingrimsson and Thordarson (2001); Stefánsson and Gunnlaugsson (1985); Tareke (2002); Kewiy (2013); Hartanto (2005): Bawasu (2014); Sorey and Colvard (1994) and Abad (2003).
2. Sampling pressures provided by ISOR, Orkuveita Reykjavikur, and Ormat. Pressure (bar) = Gauge Pressure (bar-g) + 1.
3. Reservoir enthalpy determined using steam tables for pure water (Wagner and Kretschmar, 2008), at the liquid-vapor saturation corresponding to the reservoir temperature (Reykjanes and Svartsengi); and are discharge enthalpies measured at the well head (Nesjavellir and Hellisheidi).
4. Well head liquid and steam enthalpies determined using steam tables for pure water (Wagner and Kretschmar, 2008), constrained by the two-phase liquid-vapor curve at the sampling pressure.
5. Steam fraction (x) calculated from enthalpy (H) assuming isenthalpic discharge, where $x = (H_{reservoir} - H_{liquid}/H_{vapor} - H_{liquid})$ (Henley, 1984).
6. Temperature data for Puna wells were not available, so a value of 350 °C was used to approximate temperatures of 343 °C, 354 °C, 350 °C, 354 °C, and 360 °C reported in adjacent wells KS-1, KS-1A, KS-3, KS-8, and HGP-A, respectively, by Sorey and Colvard (1994).
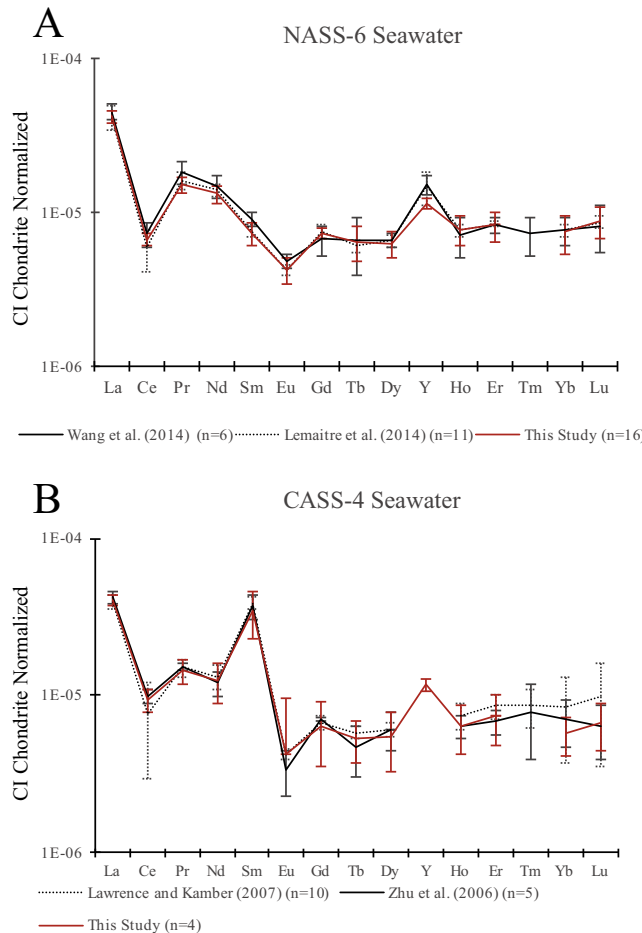
Fig. 3. Chondrite normalized (McDonough and Sun, 1995) REE values measured in the NASS-6 and CASS-4 seawater standards (2SD error bars) compared to values published by (Lawrence and Kamber, 2007; Lemaitre et al., 2014; Wang et al., 2014; Zhu et al., 2006).

(bright white phases in supplemental file A4 Figure D), an Fe-oxide phase that could not be characterized definitively by EMP, and in one location, several ~1 μm by 3 μm grains of an unidentified Zr-phase. The composition is similar to fluorapatite reported from Svartsengi, with a F/(F + Cl + OH) that ranges from 0.45 to 0.82. Reykjanes fluorapatite includes measurable, although trace, concentrations of cerium and neodymium (supplemental file A5). Fluorapatite has also been identified previously in geothermal drill cuttings from the Svartsengi geothermal system, with an F/(F + Cl + OH) ratio ranging from 0.65 to 0.95 (Lonker et al., 1993).

4.4. Results for reconstructed fluids

Q/K saturation diagrams derived from steam-loss corrected RN-24, SV-7, and HE-4 samples closely replicate observed secondary minerals at saturation indices that intersect at maximum measured reservoir temperatures (Fig. 6). Equilibrium with fluorapatite at the predicted Q/K temperature results in very low (nmol/kg) PO_4^{2-} concentrations (Table 4). Calculated concentrations for Fe and Zn assuming equilibrium control by pyrite and sphalerite, respectively, are an order of magnitude lower and

Cu assuming chalcopyrite equilibrium is two orders of magnitude lower in samples from wells RN-12 and RN-24 than the values measured in downhole samples (Table 6). Calculated concentrations of Pb are around an order of magnitude higher than those measured in downhole samples (Table 6). There are no published results for phosphorus concentrations in the studied fluids. Calculated PO_4^{2-} is at nmol/kg levels (Table 4), consistent with the very low to quantitatively absent phosphorous concentrations reported for submarine hydrothermal fluids (Wheat et al., 1996).

5. DISCUSSION

5.1. Reconciling analyzed and modeled element concentrations with previous studies

REE concentrations reported by Aggarwal et al. (1996) for Nesjavellir well NJ-11 are up to an order of magnitude higher than REE concentrations for Nesjavellir geothermal waters measured this study. Absolute REE concentrations in geothermal fluids have been shown to fluctuate over time (Sanada et al., 2006; Schmidt et al., 2010; West et al., 1992), and may account for the discrepancy. Alternatively, the discrepancy might be attributed to the standardization method

Table 4

Steam and gas loss-corrected REE values for Reykjanes peninsula, Iceland, and Puna, Hawaii, geothermal fluids; and Mg = 0 corrected REE values Middle Valley submarine hydrothermal fluids. Bold values are estimated from fixed equilibrium with specific mineral (see text for explanation).

Well		RN-12	RN-18	RN-21	RN-24	SV-07	SV-11	KS-5	KS-6W	KS-9W	KS-14E	KS-16N	HE-4	HE-5	NG-7	NG-10	Heineken Hollow	Shiner Bock
Field		Reykjanes	Reykjanes	Reykjanes	Reykjanes	Svartsengi	Svartsengi	Puna	Puna	Puna	Puna	Puna	Hellisheiði	Hellisheiði	Nesjavellir	Nesjavellir	Dead Dog	ODP
Sample date		#######	#######	#######	#######	#######	#######	#######	#######	#######	#######	#######	#######	#######	#######	#######	#######	#######
Sample ID		2E+07	2E+07	2E+07	2E+07	#######	#######	–	–	–	–	–	2014-5270	2014-5394	2014-5400	2014-5399	M3597-15	M3595-12
Sampling Pressure (bar)		29.3	24.2	27.2	25.0	15.6	8.3	17.4	17.4	16.5	17.5	18.1	9.5	9.0	14.5	14.5	–	–
[1]Temp. based on wellhead enthalpy (°C)		–	–	–	–	–	–	–	–	–	–	–	244	279	280	276	–	–
[2]Maximum Reported Measured Temp. (°C)		310	285	285	240	240	240	350	350	350	350	350	230	262	275	290	187	272
Recombined Steam Fraction		18.1%	17.3%	15.9%	16.8%	10.2%	8.3%	40.1%	40.1%	40.1%	40.1%	40.1%	15.9%	25.0%	21.0%	20.0%	–	–
[3] pH (25 °C)		3.94	4.59	4.34	4.40	4.77	4.57	6.31	5.28	5.70	5.56	5.46	6.55	5.75	6.77	6.18	5.50	5.13
pH/Temp.	(°C)	4.92/300	5.67/290	5.32/305	5.59/310	5.72/260	5.58/275	–	–	–	–	–	7.61/275	7.25/280	7.80/280	7.49/300	–	–
[4]Cl	mmol/kg	500	480	494	502	338	346	93 to 360	93 to 360	93 to 360	93 to 360	93 to 360	4.1	1.9	2.3	2.9	[*]577	[*]432
F	mmol/kg	0.011	0.010	0.010	0.010	0.010	0.009	–	–	–	–	–	0.026	0.069	<	0.057	–	–
HCO3	mmol/kg	51	27	17	31	15	21	–	–	–	–	–	6.4	21	21	9.2	–	–
HS	mmol/kg	1.5	0.66	0.63	0.67	0.41	0.63	–	–	–	–	–	2.8	1.4	6.0	4.3	–	–
SO4	mmol/kg	0.41	0.38	0.29	0.41	0.32	0.32	–	–	–	–	–	0.04	1.1	0.13	0.86	[*]0.0132	[*]0.0013
SiO2	mmol/kg	4.6	4.2	4.0	4.3	3.0	3.2	–	–	–	–	–	3.6	3.7	3.8	4.2	[*]11	
B	mmol/kg	0.6	0.6	0.6	0.7	0.6	0.6	–	–	–	–	–	–	–	–	–	–	–
NH3 (aq)	mmol/kg	1.1	0.9	0.8	0.9	0.0	0.4	–	–	–	–	–	0.6	2.8	4.5	3.1	–	–
K	mmol/kg	33	31	33	33	23	23	–	–	–	–	–	0.7	0.6	0.6	0.7	[*]20	[*]13.9
Na	mmol/kg	389	372	386	388	264	270	–	–	–	–	–	7.3	5.6	5.9	6.2	[*]416	[*]350
Ca	mmol/kg	39	33	35	35	23	24	–	–	–	–	–	0.015	0.009	0.009	0.008	[*]75.7	[*]37.5
Mg	mmol/kg	0.033	0.015	0.027	0.022	0.013	0.018	–	–	–	–	–	**7.4E-07**	**4.9E-06**	**5.8E-07**	**8.7E-07**	0	0
Mn	mmol/kg	0.042	0.016	0.021	0.023	0.002	0.002	–	–	–	–	–	–	–	–	–	[*]0.074	[*]0.150
Sr	mmol/kg	0.093	0.083	0.091	0.091	0.073	0.076	–	–	–	–	–	–	–	–	–	[*]0.282	[*]0.152
Ba	mmol/kg	0.057	0.048	0.055	0.055	0.011	0.012	–	–	–	–	–	–	–	–	–	–	–
Al	µmol/kg	1.9	2.7	3.2	2.7	2.5	2.3	–	–	–	–	–	48	53	52	60	–	–
Fe	µmol/kg	**36**	**3.1**	**49**	**18**	**0.3**	**0.8**	–	–	–	–	–	**0.28**	**0.03**	**0.27**	**0.18**	[*]20	[*]361
Cu	µmol/kg	**3.9**	**0.3**	**1.7**	**1.1**	**0.1**	**0.2**	–	–	–	–	–	**0.03**	**0.05**	**0.11**	**0.03**	[*]0.37	[*]2.8
Zn	µmol/kg	**110**	**3.9**	**52**	**19**	**0.8**	**2.3**	–	–	–	–	–	**0.42**	**0.59**	–	–	[*]1.2	[*]2.8
Pb	µmol/kg	**20**	**0.6**	**9.7**	**3.8**	**0.1**	**0.2**	–	–	–	–	–	**0.05**	**0.07**	**0.13**	**0.19**	[*]101E3	[*]158E3
PO4	nmol/kg	–	**0.3**	–	**0.8**	**0.5**	**0.8**	–	–	–	–	–	**0.66**	**3.22**	–	**1.0**	–	–
Y	pmol/kg	<	<	<	<	<	<	<	33	<	17	17	<	<	<	<	1696	124
La	pmol/kg	226	195	106	100	70	77	<	20	10	15	25	34	32	31	30	2785	832
Ce	pmol/kg	6.2	13	16	9.2	9.0	*7.0*	*5.0*	9.1	7.7	7.9	14	6.8	10	*3.7*	*3.7*	3605	1271
Pr	pmol/kg	<	*1.3*	*1.3*	<	<	<	<	<	<	<	*1.5*	<	<	<	<	365	127
Nd	pmol/kg	<	<	<	<	<	<	<	7.2	<	<	5.8	<	<	<	<	1333	367
Sm	pmol/kg	*1.3*	*1.9*	*1.9*	*1.5*	<	<	<	3.3	<	2.5	*1.5*	<	<	<	<	223	18
Eu	pmol/kg	25	26	36	32	7.8	9.4	18	144	32	60	58	*0.4*	<	<	<	4106	129
Gd	pmol/kg	<	<	<	<	<	<	<	<	<	<	<	<	<	<	<	305	46
Tb	pmol/kg	<	*0.2*	*0.3*	*0.2*	<	<	<	<	<	<	<	<	<	<	<	31	3
Dy	pmol/kg	<	<	<	<	<	<	<	<	<	<	<	<	<	<	<	150	10
Ho	pmol/kg	<	<	<	<	<	<	<	<	<	<	<	<	<	<	<	29	2
Er	pmol/kg	<	<	<	<	<	<	<	<	<	<	<	<	<	<	<	84	5
Tm	pmol/kg	–	–	–	–	–	–	–	–	–	–	–	–	–	–	–	–	–
Yb	pmol/kg	3.2	2.9	4.6	2.9	0.7	0.7	<	<	<	<	<	<	<	<	<	68	5.8
Lu	pmol/kg	1.1	1.1	1.9	1.2	0.3	0.3	<	0.6	<	0.3	0.3	<	<	<	<	11	1

– Not analyzed. A Tm spike was added to each sample to verify REE recovery during the preconcentration process.

[*]Middle Valley endmemebr vent fluid compositions from Cruse et al. (2008).

Bold Value obtained by equilibration with a mineral at the specified temperature.

Mg = tremolite (Hellisheidi and Nesjavellir only); Fe = pyrite; Cu = chalcopyrite; Zn = sphalerite; Pb = galena; HPO4-=fluorapatite (Iceland) or hydroxyapatite (Middle Valley).

< Value below the method detection limit. For REE, the detection limit is equivalent to 6[*]SD of 16 replicate measurements of the NASS-6 seawater standard.

italics REE value below conservative detection limit of 6 [*] SD replicate NASS-6 measurements, but above less conservative detection limit of 3 [*] SD.

1 Estimated using measured total wellhead enthalpy corresponding to a temperature on the 2-phase boundary for pure water.

2 Reservoir temperatures from: Fridriksson and Giroud (2008); Bjornsson et al. (1998); Steingrimsson and Thordarson (2001); Stefánsson and Gunnlaugsson (1985); Tareke (2002); Kewiy (2013); Hartanto (2005): Bawasu (2014); Abad (2003); Cruse et al. (2008). Temperature data for Puna wells were not available, so a value of 350 °C was used to approximate temperatures of 343 °C, 354 °C, 350 °C, 354 °C, and 360 °C reported in adjacent wells KS-1, KS-1A, KS-3, KS-8, and HGP-A, respectively, by Sorey and Colvard (1994).

3 pH (25 °C) values for Icelandic geothermal fluids reconstructed for gas loss. Middle Valley values are endmember fluids (extrapolated to Mg = 0) from Butterfield et al. (1994). Puna values are for the liquid fraction only, as gas data were not available to reconstruct fluid pH.

4 Cl values for Puna are the range from the HGP-A test well reported by West et al. (1992).

used by Aggarwal et al. (1996), which used digested rock solutions not matched to the fluid REE concentrations.

Cu, Zn, Fe and Pb concentrations calculated for the Reykjanes geothermal system in this study (Table 4) are at odds with downhole concentrations of these elements measured in many of the same geothermal wells by Hardardóttir et al. (2009). Observations of chalcopyrite and sphalerite scale on pipes in the Reykjanes geothermal system, minerals that control dissolved Cu and Zn concentrations, indicate that precipitation of these minerals is not kinetically inhibited and equilibrium assumptions are valid. Therefore, Cu and Zn concentrations set by equilibrium with chalcopyrite and sphalerite should represent maximum downhole concentrations in Reykjanes fluids. Fe concentrations in deep Reykjanes fluids are likely controlled by pyrite, based on the common occurrence of pyrite in drill cutting samples (Libbey and Williams-Jones, 2016; Marks et al., 2010). Therefore, Fe concentrations set in equilibrium with pyrite should represent the maximum possible downhole Fe concentration. Contrary to findings for Cu, Zn and Fe, the concentrations of Pb calculated in equilibrium with galena in this study are higher than those reported by Hardardóttir et al. (2009) for downhole samples. Galena is a common well scale mineral in Reykjanes geothermal wells (Hardardóttir et al., 2009; Hardardóttir et al., 2013) and likely controls Pb concentrations on boiling. The higher calculated Pb concentrations assuming galena equilibrium in deep fluids, therefore, reflects a maximum potential that exceeds true values.

Redox conditions and pH are important controls on metal transport in hydrothermal solutions, where lower pH leads to higher metal concentrations (Seyfried Jr and Bischoff, 1977; Seyfried Jr and Ding, 1993a). One explanation for the discrepancy between calculated and measured Cu and Fe in Reykjanes fluids may be the assumptions used to calculate redox conditions and pH in our models. However, the higher calculated Pb concentration than measured by Hardardóttir et al. (2009) suggests that pH is not overestimated in the models. One possibility for the discrepancy between measured and dissolved metal concentrations is that the assumption of sulfate-sulfide equilibrium may not be valid. Alternatively, it is notable that measured Fe and Cu reported by Hardardóttir et al. (2009) for Reykjanes fluids exceed values measured in submarine hydrothermal fluids that are typically more acidic and higher temperature, and the lack of a blank used in the study should be considered.

5.2. Factors controlling fluid REE concentrations

The primary finding of this study is that REE concentrations in boiled basalt-hosted geothermal fluids are lower than those in any high temperature (>240 °C) submarine hydrothermal fluid encountered thus far. The similarity of rocks in the Reykjanes geothermal system to oceanic crust (e.g. Fowler and Zierenberg, 2016; Marks et al., 2010) precludes rock type as a major control on the REE concentrations. This assertion is supported by studies of REE in submarine fluids from Manus back-arc basin, where rock
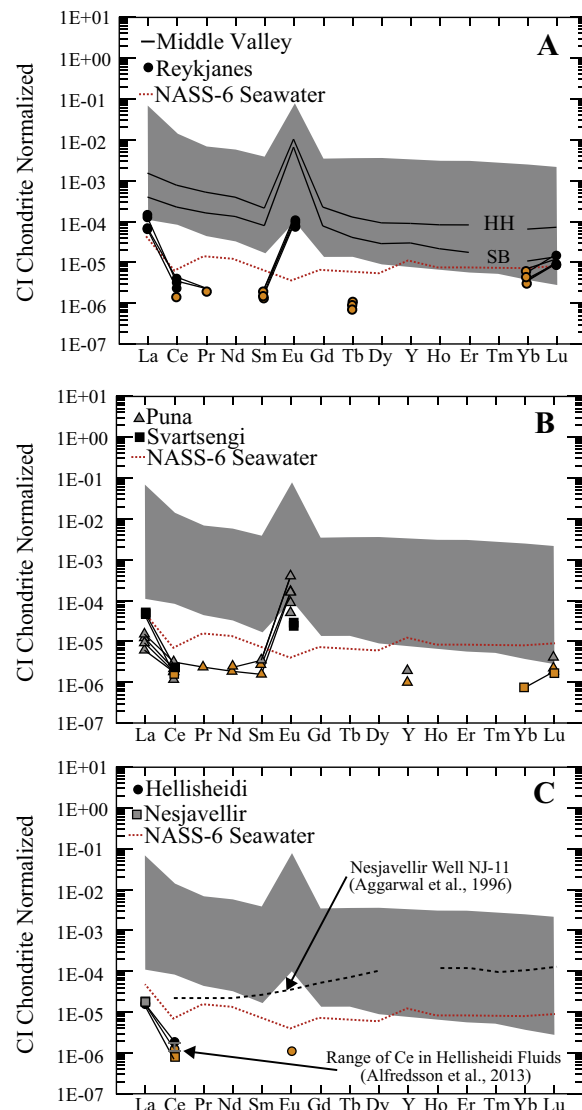
Fig. 4. Chondrite normalized (McDonough and Sun, 1995) REE patterns for fluids measured in this study. (A) Seawater-recharged terrestrial geothermal systems, (B) mixed meteoric and seawater recharged terrestrial geothermal systems, and (C) meteoric recharged terrestrial geothermal systems. Geothermal fluids (Reykjanes, Puna, Svartsengi, Hellisheidi, and Nesjavellir) are corrected for steam loss. REE values for Middle Valley submarine hydrothermal fluids are corrected by un-mixing seawater to Mg = 0, using Mg values from Cruse et al. (2008) and seawater REE values from Wheat et al. (2002). (HH = Heineken Hollow; SB = Shiner Bock). REE values reported by Aggarwal et al. (1996) for well NJ-11 at Nesjavellir and the range of Ce values for several Hellisheidi wells reported by Alfredsson et al. (2013) are indicated. Orange symbols indicate REE values below the MDL (6*SD of 16 replicate measurements of the NASS-6 seawater standard) but above 3*SD of 16 replicate measurements of the NASS-6 seawater standard. The shaded area is the range of values for REE in submarine hydrothermal fluids corrected to Mg = 0, from: (Bao et al., 2008; Bau and Dulski, 1999; Craddock et al., 2010; Douville et al., 1999; James et al., 1995; Klinkhammer et al., 1994; Michard and Albaréde, 1986; Michard et al., 1984; Mitra et al., 1994). (For interpretation of the references to colour in this figure legend, the reader is referred to the web version of this article.)

Table 5
Analytical results for well scale samples from Reykjanes well RN-9 surface pipes.

Well	RN-9	RN-9	RN-9	RN-9	RN-9
Sample	1	2	3	4	28
Depth (m)	Surface Pipe	Surface Pipe	Surface Pipe	Surface Pipe	Surface Pipe
Major elements (Weight % Oxide)					
SiO_2	82.45	85.84	81.78	76.21	45.21
Al_2O_3	1.43	0.86	1.3	3.07	2.65
Fe_2O_3	4.03	4.21	4.23	4.31	6.18
MnO	0.464	0.483	1.058	0.86	0.549
MgO	0.8	0.93	0.45	0.33	0.2
CaO	0.33	0.31	0.5	0.79	1.2
Na_2O	0.46	0.57	0.9	1.1	0.9
K_2O	0.38	0.25	0.44	0.74	0.55
TiO_2	0.001	0.002	0.001	0.002	0.001
P_2O_5	0.01	< 0.01	0.01	0.02	< 0.01
LOI	6.21	5.25	7.57	9.25	18.95
Total	96.57	98.71	98.24	96.68	76.39
Trace elements (ppm)					
Cu	4590	1990	3550	3470	> 10,000
Zn	> 10,000	> 10,000	> 10,000	> 10,000	> 10,000
Pb	3890	1590	3100	3400	<5000
Sc	< 1	< 1	< 1	< 1	< 1
Y	< 0.5	< 0.5	< 0.5	0.6	< 0.5
La	0.32	1.08	0.09	4.03	1.68
Ce	0.67	1.98	0.14	7.55	4.27
Pr	0.08	0.2	0.02	0.5	0.31
Nd	0.24	0.7	0.07	1.49	1.03
Sm	< 0.01	0.08	< 0.01	0.19	0.16
Eu	< 0.005	0.023	< 0.005	0.056	0.042
Gd	0.01	0.07	< 0.01	0.18	0.09
Tb	< 0.01	< 0.01	< 0.01	0.02	0.01
Dy	0.02	0.06	< 0.01	0.12	0.06
Ho	< 0.01	< 0.01	< 0.01	0.02	< 0.01
Er	< 0.01	0.03	< 0.01	0.06	0.02
Tm	< 0.005	< 0.005	< 0.005	0.008	< 0.005
Yb	0.01	0.03	< 0.01	0.04	0.02
Lu	< 0.002	0.005	0.002	0.006	0.004

Analyses performed by Actlabs (Ontario, Canada).
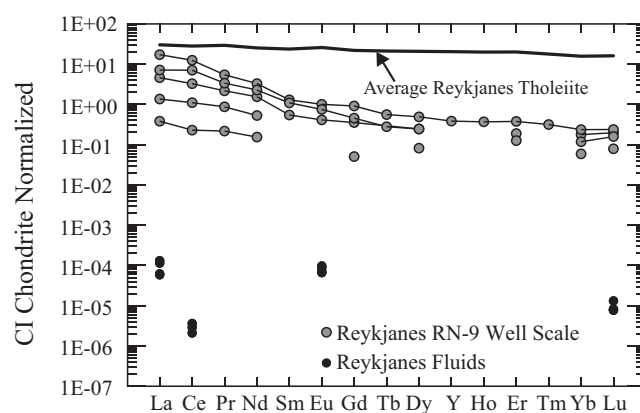
Fig. 5. Chondrite normalized (McDonough and Sun, 1995) REE values for well scale from surface pipes connected well RN-9 in the Reykjanes geothermal system. REE values for typical Reykjanes trace element enriched tholeiitic basalts (Fowler and Zierenberg, 2016) and fluids (this study) are also indicated.
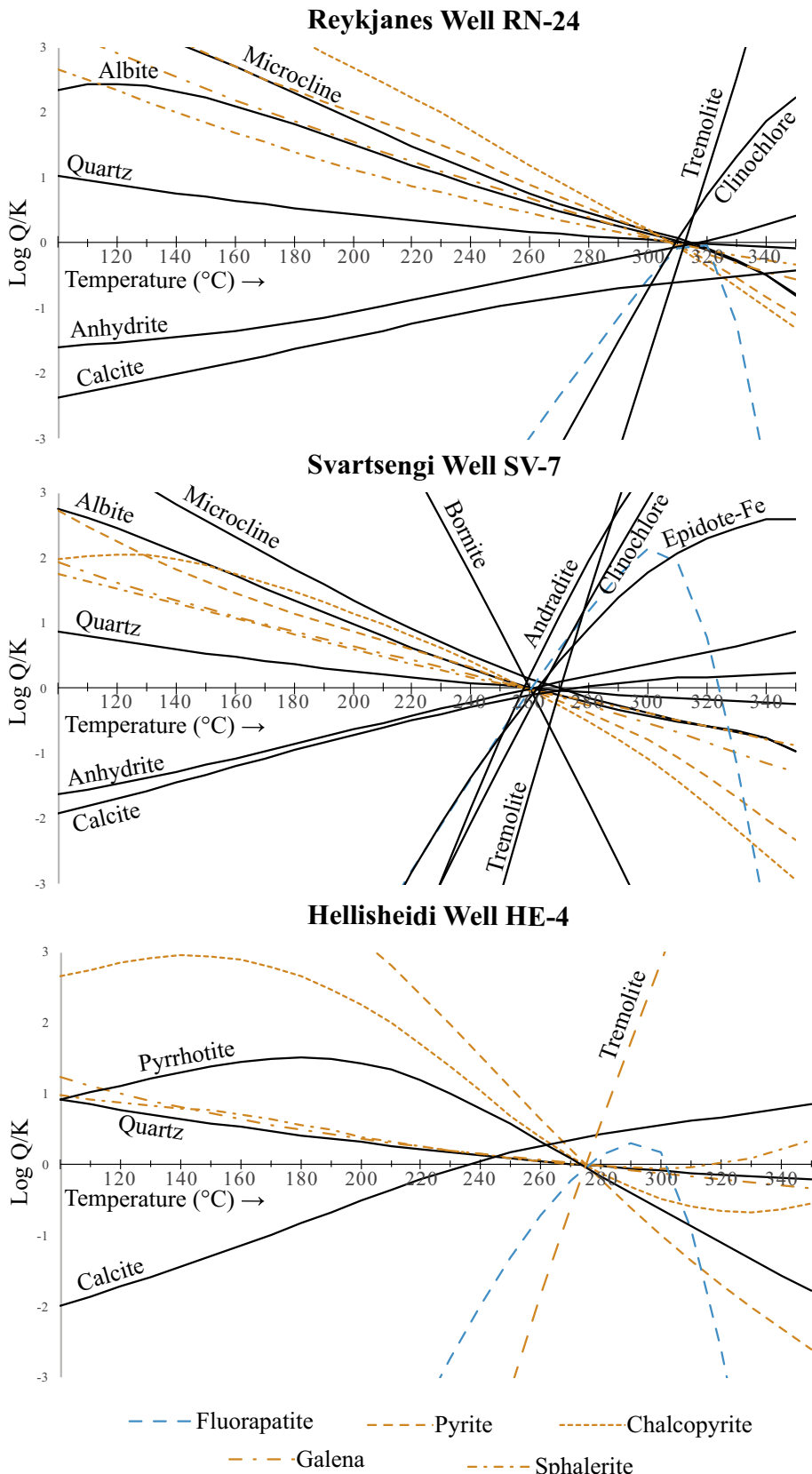
Fig. 6. Q/K diagrams for reconstructed fluids calculated using SOLVEQ-XPT. Dashed lines represent minerals used to set fluid component concentrations by fixing equilibrium with specific minerals at the calculated fluid equilibrium temperature (see 'Methods' for details).

Table 6
Calculated vs. measured Fe, Cu, Zn, and Pb concentrations in Reykjanes fluids.

Well	Field	Method	Fe μmol/kg	Cu μmol/kg	Zn μmol/kg	Pb μmol/kg
RN-12	Reykjanes	[1]Calculated	36	3.9	110	20
		[2]**Measured**	**430**	**261**	**393**	**1.3**
RN-21	Reykjanes	[1]Calculated	49	1.7	52	10
		[2]**Measured**	**2431**	**207**	**189**	**1.4**

1. This study: details for fluid reconstruction and equilibrium assumptions are given in footnotes to Table 2.
2. Downhole sample reported by Hardardóttir et al. (2009).

type is variable and fluid chemistry principally controls absolute REE concentrations (Craddock et al., 2010).

Rock leaching experiments suggest REE in geothermal and hydrothermal fluids are leached from minor phosphate phases along grain boundaries and interstitial to major minerals rather than from plagioclase dissolution (Bach and Irber, 1998; Kikawada et al., 1995; Shibata et al., 2006). Experiments simulating the reaction of seawater with gabbro indicate that variations in fluid flux and rock leaching time are required to modify REE_N patterns, and that sustained low pH fluids resulting from high water-rock ratios are most effective for leaching REE from rocks (Beermann et al., 2017). The transport and deposition of REE is controlled by the stability of aqueous species and differing affinities for REE in the structures of secondary minerals (Haas et al., 1995; Migdisov and Williams-Jones, 2014). REE mobilization is facilitated by the availability of the transporting ligands chloride and sulfate, and REE removal from solution is typically controlled by depositional ligands including fluoride, carbonate, and phosphate (Migdisov et al., 2016). At relatively high chloride activities, chloride is effective at transporting REE because the stability of REE-chloride species exceeds that of HCl, which is a strong acid and remains largely dissociated at temperature, pressure, and pH conditions typical of most natural hydrothermal systems (Migdisov and Williams-Jones, 2014).

The Reykjanes geothermal system is like submarine hydrothermal systems with regard to factors that control REE sources and transport. The major element composition of deep Reykjanes geothermal fluids is comparable to typical basalt-hosted submarine hydrothermal fluids (Hardardóttir et al., 2009). Water-rock ratios (w/r) calculated for the Reykjanes geothermal system based on strontium and oxygen isotope measurements of altered rocks (w/r of 0.3–10.2 and 0.4–4.3, respectively; Marks et al., 2015), are comparable to those estimated for many basalt-hosted submarine hydrothermal systems and ophiolites; e.g. 0.55–0.66 for Hess Deep (Kirchner and Gillis, 2012), <1–5 for Hole 504B (Friedrichsen, 1985; Kawahata et al., 1987), 1.5 for EPR 21°N (Albarède et al., 1981), 5.4 for EPR 13°N (Michard et al., 1984), 0.04 to 4.2 Samail ophiolite (Gregory and Taylor, 1981) and 15 for the Troodos ophiolite (Spooner et al., 1977). Maximum temperatures and pressures encountered in the 4.5 km deep Iceland Deep Drilling Project well IDDP-2 drilled in the Reykjanes system exceed the critical point of seawater-salinity fluids and flowing fluid is present (Friðleifsson et al., 2017), conditions that persist in the roots of many submarine hydrothermal systems (Gillis, 2002; Nehlig et al., 1994; Richardson et al., 1987; Seyfried Jr and Ding, 1993b; Von Damm et al., 2003). In addition, rock types and the crustal structure encountered at depth in the Reykjanes geothermal system are comparable to rocks drilled from oceanic crust that formed at fast-spreading ridges (Fowler and Zierenberg, 2016; Fowler et al., 2015; Friðleifsson et al., 2017; Marks et al., 2010). The calculated pH of Reykjanes geothermal fluids reconstructed for steam loss ($pH_{(25°C)}$ 3.97 in RN-12 to 4.59 in RN-18) is at the high end, but comparable to the range of values calculated for many basalt-hosted submarine hydrothermal fluids (e.g. $pH_{(25°C)}$ 2.1–4.5; Douville et al., 1999). The above considerations suggest deep Reykjanes fluids should have REE concentrations within the range of values typical for submarine hydrothermal fluids.

The Reykjanes geothermal system differs from submarine hydrothermal systems in that it is terrestrial and maximum fluid temperatures are controlled by the pressure dictated by geothermal energy production considerations, a pressure substantially lower than for typical submarine systems where pressure is controlled by the weight of overlying seawater (e.g. 23.2–28.3 bar well pressure at Reykjanes compared to greater than 200 bar for typical submarine systems). For terrestrial geothermal systems where fluids are not produced for energy, the maximum fluid temperature is dictated by atmospheric pressure at the elevation of venting. Kaasalainen et al. (2015) proposed that many trace metals are removed from Icelandic geothermal fluids during boiling or cooling along flow paths and incorporated into secondary minerals. Scale precipitates rapidly in Reykjanes geothermal wells at a rate of 1.5–11 mm/year (Hardardóttir et al., 2005). Well RN-9, the source of scale analyzed in this study, was operated at an average fluid production of $\sim1.4 \times 10^9$ kg/year, and precipitated an estimated 2000–3000 kg/year of scale in surface piping alone (Hardardóttir et al., 2010). Values for scale mass production rate, fluid production rate, and the REE concentration in well scale samples provides a basis to estimate REE removed per kilogram of fluid into surface pipe scale (Table 7). Well scale also forms downhole in the boiling zone (Hardardóttir et al., 2013), but REE concentrations in downhole scale and mass production rates are not available, so are not included in Table 7 calculation. As such Table 7 calculation, which is based on the REE content of surface piping, underestimates total REE removal from fluids into well scale solids. Table 7 results are useful for

Table 7
Estimated picomole of REE per kg of fluid incorporated into surface piping scale in Reykjanes geothermal well RN-9 compared to REE in a typical boiled Reykjanes fluid (RN-24 fluid).

Well	RN-9 Scale	RN-9 Scale	RN-9 Scale	RN-9 Scale	RN-9 Scale	RN-24 Fluid
Sample	1	2	3	4	28	(pmol/kg)
Y	<	<	<	9.64	<	<49.5
La	3.3	11.1	0.9	41.45	17.3	**100**
Ce	6.8	20.2	1.4	76.98	43.5	**9.2**
Pr	0.8	2.0	0.2	5.07	3.1	<3.3
Nd	2.4	6.9	0.7	14.76	10.2	<16.4
Sm	<	0.8	<	1.81	1.5	<3.6
Eu	<	0.2	<	0.53	0.4	32.0
Gd	0.1	0.6	<	1.64	0.8	<2.2
Tb	<	<	<	0.18	0.1	<1.2
Dy	0.2	0.5	<	1.05	0.5	<5.8
Ho	<	<	<	0.17	<	<1.6
Er	<	0.3	<	0.51	0.2	<5.1
Tm	<	<	<	0.07	<	–
Yb	0.1	0.2	<	0.33	0.2	<6.4
Lu	<	0.0	0.0	0.05	0.0	**1.2**

Estimated picomol REE incorporated into scale per 1 kg fluid compared to the measured REE concentration in fluid.
– Not Measured.
< Below the stated detection limit, which pertains to the fluid sample only.
Values calculated from $[((2000 \text{ kg scale/year})/(1.4 * 10^9 \text{ kg fluid/year})] * [\text{pmol/kg REE in scale}]$.
Measured REE values in RN-24 fluid (pmol/kg) shown for comparison.

showing that several Reykjanes scale samples require a significant fraction, or more, of REEs that are available in boiled RN-24 fluids. Thus, well scale solids are an important REE sink and downhole fluids must have higher REE concentrations than measured at the wellhead. While sulfide-rich scales are typical of low pH and saline geothermal fluids, carbonate scale is an important sink for REE in terrestrial geothermal systems with neutral to high pH such as sediment-hosted geothermal fluids in the Kizildere geothermal field, Turkey (Möller et al., 2008). Such scales are predicted to form in the boiling models presented for the near-neutral pH Hellisheidi and Nesjavellir geothermal systems in Iceland (Fig. 7).

5.3. CHIM-XPT boiling models

Isenthalpic boiling models completed using CHIM-XPT calculate supersaturation of a series of Ca-Fe-Mg silicate minerals, however these minerals are not typically observed in geothermal well scale samples because of slow formation kinetics (Spycher and Reed, 1989). Kinetic controls on the formation of silicate minerals in geothermal well scale has been documented in the Ngatamariki geothermal system in New Zealand, where epidote, wairakite, prehnite and quartz formed only after prolonged (at least 10–472 days) well shut-in conditions (Browne et al., 1989). To accommodate slow kinetics of silicate formation in the CHIM-XPT models, silicate minerals including garnet, epidote, prehnite, pyroxene, amphibole, chlorite group, smectite group, mica, feldspar, and silica polymorphs (except amorphous silica) were suppressed from forming in the models. Iron silicates have been documented in well scale samples from Icelandic geothermal systems (Ármannsson and Hardardóttir, 2010;

Kristmannsdóttir, 1989), so we accommodate iron-silicate formation in our models by allowing the Fe-rich smectite nontronite-Ca to precipitate.

5.4. Well scale predictions from CHIM-XPT boiling models

Deep, single-phase Reykjanes geothermal fluids that persist at temperatures exceeding 270 °C boil upon depressurization and precipitate pyrrhotite, sphalerite, galena, pyrite, chalcopyrite, hematite, and anhydrite in the downhole boiling zone (Hardardóttir et al., 2013). At pressures lower than 20 bar, bornite, amorphous silica, and an unidentified Fe-silicate clay mineral form in surface pipes (Hardardóttir et al., 2005). In good agreement with observed Reykjanes well scale minerals, the CHIM-XPT boiling model calculates precipitation of anhydrite, sphalerite, galena, pyrite, hematite, bornite, nontronite-Ca, and amorphous silica. In addition, monazite-Y (YPO_4) and $Y(OH)_{3(s)}$ precipitate on boiling. In the REE-free boiling model, fluorapatite replaces monazite-Y as the precipitated phosphate mineral (Fig. 7A).

Boiled Svartsengi geothermal fluids primarily precipitate calcite and amorphous silica scale in wells, along with minor unspecified metal sulfides (Kristmannsdóttir, 1989; Lindal, 1989). The CHIM-XPT boiling model for well SV-7 produces a similar scale mineral assemblage as that observed in and calculated for Reykjanes well RN-24: calcite, sphalerite, galena, pyrite, chalcopyrite, bornite, nontronite-Ca, and amorphous silica. In addition, fluorapatite, monazite-Y, monazite-Ce ($CePO_4$), monazite-La ($LaPO_4$), and $Y(OH)_{3(s)}$ precipitate on boiling. As in the RN-24 model, fluorapatite replaces monazite-Y, -Ce, and La as the most supersaturated phosphate mineral in the REE-free model (Fig. 7B).
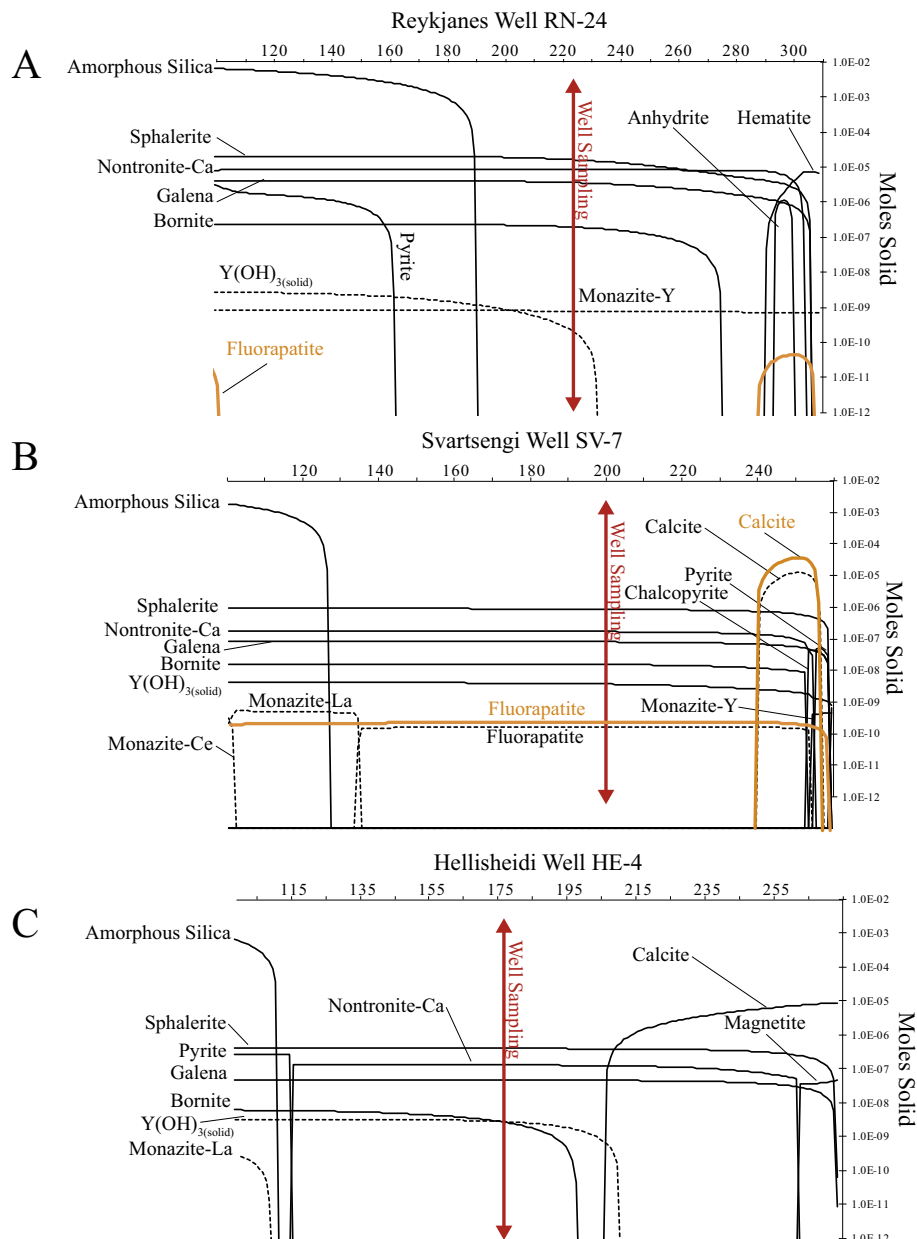
Fig. 7. A–C: Results for CHIM-XPT boiling models showing moles of solids produced per kilogram fluid as a function of temperature. Results are shown for sample RN-24; results for samples SV-7 and HE-4 are provided as supplemental file A6. Boiling models were calculated using (1) the average for submarine hydrothermal fluids for which yttrium data are available (i.e. Bao et al., 2008; Douville et al., 1999; Douville et al., 2002) (i.e. REE-bearing), and (2) no dissolved REE (i.e. REE free). Precipitated minerals unique to the REE-bearing model are indicated with dashed lines; precipitated minerals in the REE-free model are indicated by solid orange lines. (For interpretation of the references to colour in this figure legend, the reader is referred to the web version of this article.)

Hellisheidi geothermal fluids precipitate amorphous silica scale, trace Fe-sulfides, and trace Fe-oxides (Meier et al., 2014). No data on downhole scale is available specifically for the Hellisheidi and Nesjavellir geothermal systems, but in general high-temperature meteoric water-recharged Icelandic geothermal systems commonly precipitate calcite/aragonite, silica, Fe-sulfide (pyrite and pyrrhotite), Fe-silicates, magnetite, and hematite (Kristmannsdóttir, 1989). The HE-4 boiling model results are broadly compatible with typical Icelandic geothermal

scale minerals, and includes calcite, magnetite, nontronite-Ca, amorphous silica, and pyrite. The CHIM-XPT model also calculates precipitation of sphalerite, galena, bornite, Y(OH)$_{3(s)}$ and monazite-La (Fig. 7C). Calculated Cu-, Zn- and Pb sulfides in scale from meteoric recharged systems reflects the model constraints of setting Cu, Zn and Pb in equilibrium with chalcopyrite, sphalerite, and galena, respectively. The outcome is the maximum potential Cu, Zn and Pb concentrations, which probably over-estimate real-world concentrations because lower pH fluids than those at

Hellisheidi and Nesjavellir are required to efficiently leach these elements from host rocks (e.g. Seyfried Jr and Bischoff, 1977). Reactive fluids, such HCl-bearing ones, are also required to mobilize significant REE from host rocks (Beermann et al., 2017), therefore the average value of REE in more acidic submarine hydrothermal fluids probably overestimate REE in the more alkaline Hellisheidi and Nesjavellir fluids. In the REE-free model, no phosphate minerals are calculated to precipitate on boiling (Fig. 7C).

5.5. Aqueous REE speciation on boiling

Aqueous LREE, Eu, and HREE speciation vary with progressive boiling, and differ for fluids with and without a seawater component (Fig. 8 and supplemental file A6). At the onset of boiling, the major REE species in the samples with a seawater component (RN-24 and SV-7) are REE(III)-hydroxides, followed by LREE(III)-chloride complexes. Eu differs from other REE in that it is exclusively Eu(II), and the major aqueous species is $Eu(II)Cl^+$ followed by the simple hydrated Eu(II) ion and Eu(II)-carbonate and bicarbonate species (Fig. 8A–C). In the higher pH meteoric-recharged Hellisheidi system, REE are calculated to be near exclusively complexed with hydroxides at the onset of boiling, and Eu is predominantly present as oxidized Eu(III) complexed with hydroxides (supplemental file A6).

The relative proportions of LREE(III)-chloride, LREE(III)-fluoride, and REE(III) simple hydrated ions increase at the expense REE(III)-hydroxides on progressive boiling of the RN-24 and SV-7 samples. The proportion of the $Eu(II)Cl^+$ species also increases at the expense of the Eu(II) ion and Eu(II)-carbonate and bicarbonate species (Fig. 8A–C). Increases in the proportion of $La(III)Cl^{++}$ and $Eu(II)Cl^+$ relative to other REE are particularly apparent throughout boiling of the RN-24 and SV-7 samples. In the HE-4 sample, REE (III) hydroxide species remain dominant throughout the boiling models. Other REE ligand complexes increase in proportion on progressive boiling of the HE-4 sample, particularly REE bicarbonate and carbonate species, however these complexes remain an insignificant proportion of the total REE in solution (supplemental file A6).

Available thermodynamic data for the full REE suite of hydroxide species are extrapolated to hydrothermal temperatures from measurements made at 25 °C (Haas et al., 1995). The only experimental data for REE hydroxide complexes is limited to Nd-hydroxide formation constants (Wood et al., 2002), and suggest that the (Haas et al., 1995) Nd-hydroxide formation constants are overestimated by orders of magnitude (Migdisov et al., 2016). Disagreement between experimental and extrapolated REE hydroxide thermodynamic data is minimized when studying acidic fluids where chloride and fluoride REE complexes dominate over REE hydroxide complexes. In near-neutral high-temperature fluids, such as those presented in this study, potential errors in REE hydroxide formation constants may result in underestimation of the importance of competing REE-ligand complexes, particularly for the alkaline HE-4 sample. The lack of experimentally verified data

for REE hydroxide complexes at elevated temperatures is an important data gap, and, the extrapolations of Haas et al. (1995) provide the best currently available approximation for modeling REE hydroxide speciation until experimentally verified data become available. Modifications to hydroxide thermodynamic data in the future may influence conclusions about the dominant REE aqueous species, but will not greatly influence conclusions about relative changes in proportions REE species on progressive boiling; i.e. REE-ligand complexes increase in strength relative to REE hydroxide species.

Variations in aqueous speciation and species activity on progressive boiling reflect the effects of changes in the physical properties of the solution upon changes in the pressure and temperature conditions. Partitioning of acid gases (e.g. H_2S and CO_2) into the vapor phase on boiling leads to pH increases in the RN-24 sample from pH $5.5_{(310°C)}$ to pH $6.3_{(100°C)}$; from pH $5.7_{(260°C)}$ to pH $7.0_{(100°C)}$ in the SV-7 sample, and from pH $7.6_{(275°C)}$ to pH $8.6_{(100°C)}$ in the HE-4 sample. In addition to pH effects, exsolving a gas phase that includes water vapor increases the concentration of components in the residual liquid. While increased pH favors formation of hydroxidated REE, the increased concentration of components in the residual liquid outcompetes the pH effect and increases the abundance of REE-ligand complexes. The increased strength LREE chloride complexes, particularly $La(III)Cl^{++}$ and $Eu(II)Cl^+$, provides a mechanism to produce elevated measured La_N and Eu_N in the boiled geothermal fluids with a seawater component shown on Fig. 4 (Reykjanes, Svartsengi, and Puna) by excluding La and Eu from incorporation into precipitated solid phases. This idea is consistent with water-rock reaction experiments conducted at elevated temperatures that identified elevated La and Eu concentrations relative to other REE, an attributed the result to greater strengths of La and Eu chloride complexes (Allen and Seyfried, 2005). However, the slightly elevated Lu_N concentrations observed in the boiled samples from geothermal systems with a seawater component cannot be explained by the results of aqueous speciation calculations, and suggests additional controls on REE concentrations in the boiled fluids.

5.6. Boiling model insights into controls on fluid REE

Boiling models only include thermodynamic data for pure endmember REE solids. As a result, boiling models calculate precipitation of the most saturated pure endmember REE-phosphate, which ultimately controls aqueous phosphate concentrations. The outcome is that the least soluble lanthanide-phosphate (monazite or xenotime) precipitates and prevents other REE typically present in solid solution minerals from precipitating from solution. In the models where average submarine hydrothermal fluid REE are assumed, monazite is calculated as the control on aqueous phosphate and REE concentrations (Fig. 7A–C).

The composition of natural monazite is largely restricted to a La-Ce-Nd solid solutions (Fleischer et al., 1991; Spear and Pyle, 2002). Therefore, calculated precipitation of monazite endmembers shown in Fig. 7A–C do not replicate
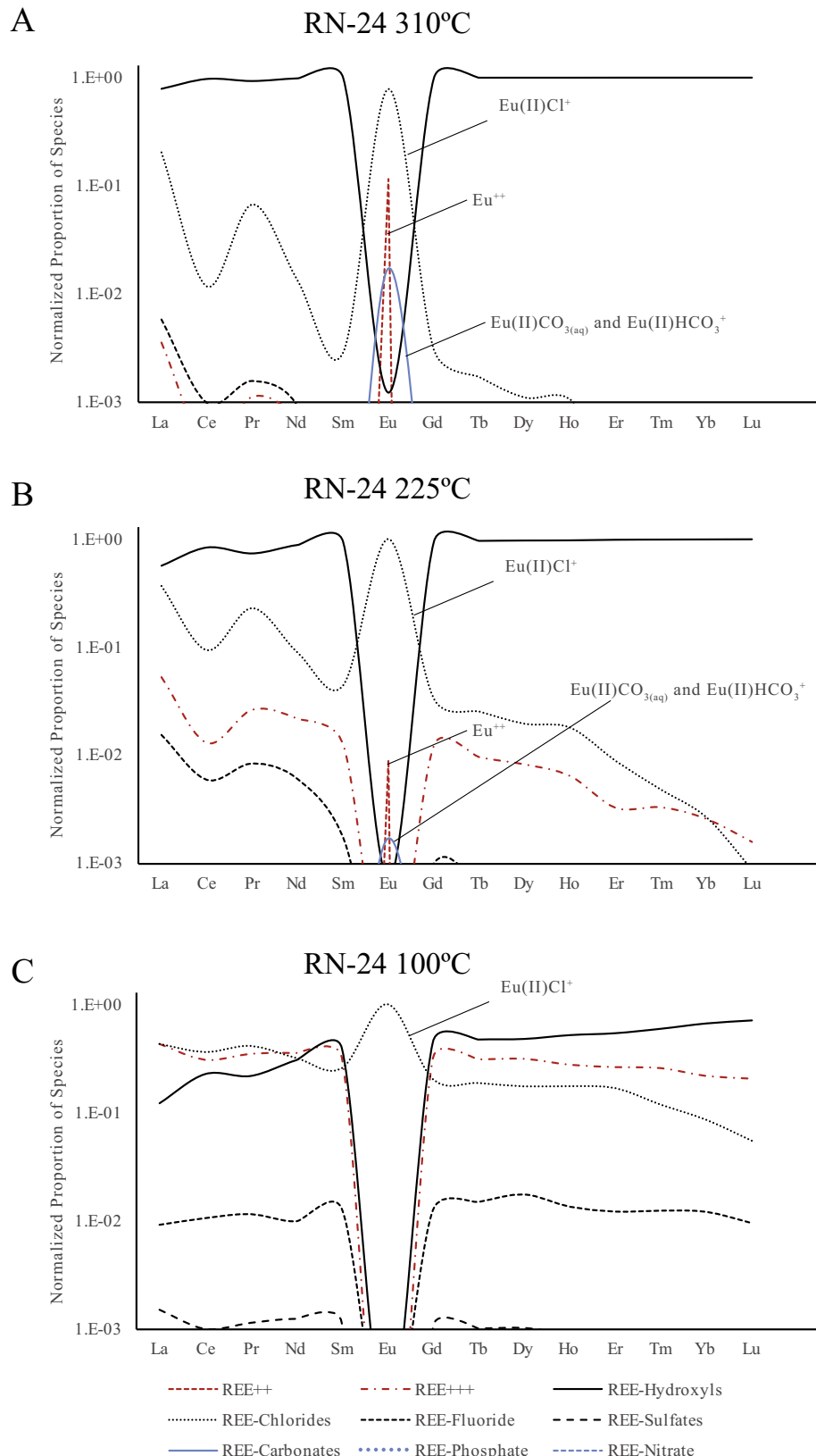
Fig. 8. A–C. REE speciation on progressive boiling of reconstructed fluids from Reykjanes well RN-24. Speciation is shown at (1) the onset of boiling at equilibration temperature identified from Q/K diagrams (i.e. Fig. 6), (2) at the approximate temperature equivalent to the sampling pressure, and (3) 100 °C. See supplemental data for figures corresponding to wells from other studied geothermal fields. Note the different y-axis scale for the HE-4 figure.

real-world conditions where aqueous lanthanide concentrations are modified by partitioning into monazite solid solution minerals. The results are, however, useful for qualitatively evaluating controls on aqueous REE by monazite supersaturation. Monazite strongly partitions LREE relative to HREE, and if monazite were the dominant phosphate controlling REE in fluids throughout boiling, we would expect a fluid depleted in LREE relative to HREE (c.f. Debruyne et al., 2016), which we do not observe. This result suggests that the average REE and Y concentrations used in the figures through 7C models probably overestimate downhole REE concentrations in the boiling models.

Overestimation of lanthanide and yttrium concentrations prevent other phosphate minerals (e.g. apatite) from forming, because the lanthanide phosphate minerals control aqueous phosphate. The REE-free models provide a means to overcome this limitation. In the REE-free models, fluorapatite replaces monazite as the least soluble phosphate mineral in the RN-24 and SV-7 samples (Fig. 7A and B), and no phosphate minerals supersaturate in the HE-4 sample (Fig. 7C). Other mineral phases in the REE-free boiling models do not differ.

If monazite supersaturation is excluded as a possible control on aqueous REE concentrations on progressive boiling, anhydrite in the RN-24 and calcite in the SV-7 models are alternative minerals that potentially control aqueous REE concentrations on boiling. Anhydrite strongly partitions REE from the aqueous phase on precipitation, and LREE and Eu(II) are excluded from the anhydrite structure when these elements are transported as chloride complexes (Bach et al., 2003; Humphris and Bach, 2005). Calcite also strongly partitions REE from geothermal fluids (Debruyne et al., 2016; Möller et al., 2008). LREE exclusion from anhydrite and calcite owing to formation of LREE chloride complexes could provide a mechanism to maintain the higher measured La and Eu concentrations in boiled geothermal fluids with a seawater (high Cl) component, but chloride complexation cannot explain higher Lu_N relative to other REE in these samples (Fig. 4). No known studies have shown higher Lu relative to adjacent REE during anhydrite or calcite formation. The general similarity of REE patterns for the Reykjanes, Svartsengi, and Puna boiled geothermal fluids suggests a common factor controls observed REE concentrations.

Apatite, which is predicted to form in both Reykjanes and Svartsengi fluids in the REE-free models (Fig. 7A and B), is important for controlling many trace element concentrations in hydrothermal fluids and strongly partitions REE (Pan and Fleet, 2002). The site preference of REE in the apatite structure is convex upward across the REE series, peaking at Nd in fluorapatite and Sm in hydroxyapatite (Fleet and Pan, 1995a; Fujimaki, 1986; Reynard et al., 1999). Modeling suggests that apatite REE partitioning characteristics decrease REE in the middle of the lanthanide series relative to La and Lu in residual silicate melts upon apatite formation (Fujimaki, 1986). Apatite/water elastic strain REE partition coefficient modeling predicts this effect influences REE in aqueous systems on apatite precipitation (Reynard et al., 1999), and the effect is more pronounced at progressively lower temperatures (supplemental file A7). The effect of fluid-apatite REE partitioning, therefore, should produce a fluid depleted in lanthanides from the middle of the series, similar to those sampled from Reykjanes, Svartsengi, and Puna. The results in supplemental file A5 show that Reykjanes apatite contains measurable REE and is important for controlling aqueous REE, however poor precision of results owing to the low REE concentrations preclude rigorous REE partition modeling. Preference of the middle REE over La and Lu in the apatite structure provides a mechanism to produce the elevated measured La_N and Lu_N concentrations observed in boiled RN-24 and SV-7 fluids, while the large positive Eu anomaly in RN-24 and SV-7 fluids is consistent with transport as a relatively stable chloride complex. Therefore, fluorapatite precipitation coupled with chloride complexation likely controls observed REE concentrations in the boiled geothermal fluids with a seawater component.

Calcite is supersaturated on boiling of the meteoric-sourced HE-4 fluid. In the absence of monazite for the HE-4 boiling model, calcite scale is the most likely candidate for controlling dissolved REE concentrations, consistent with conclusions of Möller et al. (2008) for alkaline geothermal fluids elsewhere. Published calcite/fluid REE partition coefficients range over an order of magnitude, but generally agree in that LREE are more compatible in the calcite structure than HREE (Debruyne et al., 2016). In the absence of chloride complexation, calcite/fluid partition characteristics would suggest a resulting HREE enriched fluid relative to LREE, which is not observed in the analytical results. Measured REE are largely below detection in the Nesjavellir and Hellisheidi fluids except for La, Ce and Eu. Ligand complexation of La, Ce and Eu contributes to excluding these lanthanides from the calcite structure, but is inconsistent with the very low proportion of ligand-complexed REE relative to REE-hydroxide species on progressive boiling (supplemental file A6). As discussed above, REE hydroxide species are likely significantly overestimated in the Hellisheidi models. REE-chloride, fluoride, carbonate, sulfate complexes and the free ion do increase in proportion on boiling, and if this effect is underestimated because of poor quality REE-hydroxide thermodynamic data, ligand complexation may be more important for controlling aqueous REE than calculated in the boiling models. The measured REE values indicate the next most abundant REE complexes in the HE-4 boiling models, REE-carbonate, -bicarbonate and -fluoride complexes, may be more important than the available thermodynamic data for REE-hydroxide species would suggest.

6. CONCLUSIONS

Boiling of geothermal fluids has a profound influence on aqueous REE concentrations, leading to the quantitative removal of most REE. REE are incorporated into well scale by fluorapatite precipitated from lower pH fluids with a seawater component, and by carbonate precipitated from higher pH fluids. Heterogeneous equilibrium geochemical models indicate that La(III) and Eu(II) chloride complexes become increasingly stable in Cl-rich fluids during boiling.

Thus, La and Eu persist at higher levels than other REE in the high-Cl fluids because the formation of La and Eu(II) chloride complexes inhibits partitioning of these elements into solid phases. Cl-complexation effects cannot explain the measured Lu concentrations in the boiled Cl-rich fluids. We speculate that Lu is detectable in the higher Cl fluids because it is less compatible in the fluorapatite structure than adjacent REE in the lanthanide series.

ACKNOWLEDGEMENTS

APPENDIX A. SUPPLEMENTARY MATERIAL

Supplementary data to this article can be found online at https://doi.org/10.1016/j.gca.2018.10.001.

REFERENCES

Abad, M.R.K., 2003. Reservoir parameters for well HE-5. Hellisheidi geothermal field. SW-Iceland, UNU-GTP Iceland Report 15, p. 437–463.

Aggarwal J. K., Shabani M. B., Palmer M. R. and Ragnarsdóttir K. V. (1996) Determination of the rare earth elements in aqueous samples at sub-ppt levels by inductively coupled plasma mass spectrometry and flow injection ICPMS. *Anal. Chem.* **68**, 4418–4423.

Albarède F., Michard A., Minster J. F. and Michard G. (1981) $^{87}Sr/^{86}Sr$ ratios in hydrothermal waters and deposits from the East Pacific Rise at 21 degrees N. *Earth Planet. Sci. Lett.* **55**, 229–236.

Alfredsson H. A., Oelkers E. H., Hardarsson B. S., Franzson H., Gunnlaugsson E. and Gislason S. R. (2013) The geology and water chemistry of the Hellisheidi, SW-Iceland carbon storage site. *Int. J. Greenhouse Gas Control* **12**, 399–418.

Allen D. E. and Seyfried W. E. (2005) REE controls in ultramafic hosted MOR hydrothermal systems: an experimental study at elevated temperature and pressure. *Geochimica et Cosmochimica Acta* **69**, 675–683.

Ames D. E., Franklin J. M. and Hannington M. (1993) Mineralogy and geochemistry of active and inactive chimneys and massive sulfide, Middle Valley, Northern Juan de Fuca Ridge: an evolving hydrothermal system. *Can. Mineral.* **31**, 997–1024.

Aries S., Valladon M., Polve M. and BDupre B. (2000) A routine method for oxide and hydroxide interference corrections in ICP-MS chemical analysis of environmental and geological samples. *Geostandards Newsletter* **24**, 19–31.

Ármannsson H. (2016) The fluid geochemistry of Icelandic high temperature geothermal areas. *Appl. Geochem.* **66**, 14–64.

Ármannsson H. and Hardardóttir V. (2010) Geochemical patterns of scale deposition in saline high temperature geothermal systems. In: Birkle, P., Torres-Aivarado, I.S. (Eds.), Water-Rock Interaction, pp. 133–136.

Arnórsson S. (1978) Major element chemistry of the geothermal sea-water at Reykjanes and Svartsengi, Iceland. *Mineral. Soc.* **42**, 209–220.

Arnórsson S. (1995) Geothermal systems in Iceland - structure and conceptual models – I. High temperature areas. *Geothermics* **24**, 561–602.

Arnórsson S., Bjarnason J. O., Giroud N., Gunnarsson I. and Stefansson A. (2006) Sampling and analysis of geothermal fluids. *Geofluids* **6**, 203–216.

Bach W. and Irber W. (1998) Rare earth element mobility in the oceanic lower sheeted dyke complex: evidence from geochemical data and leaching experiments. *Chem. Geol.* **151**, 309–326.

Bach W., Roberts S., Vanko D. A., Binns R. A., Yeats C. J., Craddock P. R. and Humphris S. E. (2003) Controls of fluid chemistry and complexation on rare-earth element contents of anhydrite from the Pacmanus subseafloor hydrothermal system, Manus Basin, Papua New Guinea. *Miner. Deposita* **38**, 916–935.

Bao S.-X., Zhou H.-Y., Peng X.-T., Ji F.-W. and Yao H.-Q. (2008) Geochemistry of REE and yttrium in hydrothermal fluids from the Endeavour segment, Juan de Fuca Ridge. *Geochem. J.* **42**, 359–370.

Bau M. (1991) Rare-earth mobility during hydrothermal and metamorphic fluid-rock interaction and the significance of the oxidation state of europium. *Chem. Geol.* **93**, 219–230.

Bau M. and Dulski P. (1999) Comparing yttrium and rare earths in hydrothermal fluids from the Mid-Atlantic Ridge – implications for Y and REE behaviour during near-vent mixing and for the Y: Ho ratio of Proterozoic seawater. *Chem. Geol.* **155**, 77–90.

Bawasu, M.L., 2014. Borehole stratigraphy and alteration mineralogy of well HE-6, Hellisheidi, SW-Iceland, UNU-GTP Report 9, 65–90.

Beermann O., Garbe-Schönberg D., Bach W. and Holzheid A. (2017) Time-resolved interaction of seawater with gabbro: an experimental study of rare-earth element behavior up to 475 °C, 100 MPa. *Geochim. Cosmochim. Acta* **197**, 167–192.

Bilal B. A. (1991) Thermodynamic study of $Eu^{2+}:Eu^{3+}$ redox reaction in aqueous solutions at elevated temperatures and pressures by means of cyclic voltammetry. *Zeitschrift für Naturforschung A* **46**, 1108–1116.

Bjerkgård T., Cousens B. L. and Franklin J. M. (2000) The Middle Valley sulfide deposits, northern Juan de Fuca Rdige: radiogenic isotope systematics. *Econ. Geol.* **95**, 1473–1488.

Browne P. R. L., Courtney S. F. and Wood P. C. (1989) Formation rates of calc-silicate minerals deposited inside drillhole casing, Ngatamariki geothermal field, New Zealand. *Am. Mineral.* **74**, 759–763.

Butterfield D., McDuff R. E., Franklin J. and Wheat C. G. (1994) Geochemistry of hydrothermal vent fluids from Middle Valley, Juan De Fuca Ridge. *Proceedings of the Ocean Drilling Program, Scientific Results* **139**, 395–410.

Campbell A. C., Palmer M. R., Klinkhammer G. P., Bowers T. S., Edmond J. M., Lawrence J. R., Casey J. F., Thompson G., Humphris S. E., Rona P. and Karson J. A. (1988) Chemistry of hot springs on the Mid-Atlantic Ridge. *Nature* **335**, 514.

Clifton A. E. and Kattenhorn S. A. (2006) Structural architecture of a highly oblique divergent plate boundary segment. *Tectonophysics* **419**, 27–40.

Cousens B. L., Blenkinsop J. and Franklin J. M. (2002) Lead isotope systematics of sulfide minerals in the Middle Valley hydrothermal system, northern Juan de Fuca Ridge. *Geochem. Geophys. Geosyst.* **3**, 1–16.

Craddock P. R., Bach W., Seewald J. S., Rouxel O. J., Reeves E. and Tivey M. K. (2010) Rare earth element abundances in hydrothermal fluids from the Manus Basin, Papua New

Guinea: Indicators of sub-seafloor hydrothermal processes in back-arc basins. *Geochim. Cosmochim. Acta* **74**, 5494–5513.

Craddock P. R. and Bach W. (2010) Insights to magmatic–hydrothermal processes in the Manus back-arc basin as recorded by anhydrite. *Geochim. Cosmochim. Acta* **74**, 5514–5536.

Cruse A. M. and Seewald J. S. (2006) Geochemistry of low-molecular weight hydrocarbons in hydrothermal fluids from Middle Valley, northern Juan de Fuca Ridge. *Geochim. Cosmochim. Acta* **70**, 2073–2092.

Cruse A. M., Seewald J. S., Saccocia P. J. and Zierenberg R. (2008) Hydrothermal fluid composition at Middle Valley, Northern Juan de Fuca Ridge: temporal and spatial variability. *Geophys. Monogr. Ser.* **178**, 145–166.

Davis E. E., Mottl M. J. and Fisher A. T. e. a. (1992) *Proceedings of the Ocean Drilling Program, Initial Reports 139. Ocean Drilling Program*. College Station, Texas.

Debruyne D., Hulsbosch N. and Muchez P. (2016) Unraveling rare earth element signatures in hydrothermal carbonate minerals using a source–sink system. *Ore Geol. Rev.* **72**, 232–252.

Diakonov I. I., Ragnardóttir K. V. and Tagirov B. R. (1998a) Standard thermodynamic properties and heat capacity equations of rare earth element hydroxidies:II. Ce(III)-, Pr-, Sm-, Eu (III)-, Gd-, Tb-, Dy-, Ho-, Er-, Tm-, Yb-, and Y-hydroxides. Comparison of thermochemical and solubility data. *Chem. Geol.* **151**, 327–347.

Diakonov I. I., Ragnarsdóttir K. V. and Tagirov B. R. (1998b) Standard thermodynamic properties and heat capacity equations of rare earth hydroxides: II. Ce(III)-, Pr-, Sm-, Eu(III)-, Gd-, Tb-, Dy-, Ho-, Er-, Tm-, Yb-, and Y-hydroxides. Comparison of thermochemical and solubility data. *Chem. Geol.* **151**, 327–347.

Diakonov I. I., Tagirov B. R. and Ragnarsdóttir K. V. (1998c) Standard thermodynamic properties and heat capacity equations for rare earth element hydroxides: I. La(OH)3(s) and Nd (OH)3(s). Comparison of thermochemical and solubility data. *Radiochim. Acta* **81**, 107–116.

Douville E., Bienvenu P., Charlou J. L., Donval J. P., Fouquet Y., Appriou P. and Gamo T. (1999) Yttrium and rare earth elements in fluids from various deep-sea hydrothermal systems. *Geochimica et Cosmochimica Acta* **63**, 627–643.

Douville E., Charlou J. L., Oelkers E. H., Bienvenu P., Jove Colon C. F., Donval J. P., Fouquet Y., Prieur D. and Appriou P. (2002) The rainbow vent fluids (36°14'N, MAR)- the influence of ultramafic rocks and phase separation on trace metal content in Mid-Atlantic Ridge. *Chem. Geol.* **184**, 37–48.

Fleet M. E. and Pan Y. (1995a) Crystal chemistry of rare earth elements in fluorapatite and some calc silicates. *Eur. J. Mineral.* **7**, 591–605.

Fleet M. E. and Pan Y. (1995b) Site preference of the rare earth elements in fluorapatite. *Am. Mineral.* **80**, 329–335.

Fleischer M., Rosenblum S. and Woodruff M. (1991) The distribution of lanthanides and yttrium in the minerals of the monazite family. U.S. Geological Survey Professional Paper, Open File Report 91-580, p. 125.

Fowler A.P.G. and Zierenberg R.A. (2016) Elemental changes and alteration recorded by basaltic drill core samples recovered from in-situ temperatures up to 345 °C in the active, seawater-recharged Reykjanes Geothermal System, Iceland. Geochemistry, Geophysics, Geosystems 17.

Fowler A. P. G., Zierenberg R. A., Schiffman P., Marks N. and Friðleifsson G. Ó. (2015) Evolution of fluid–rock interaction in the Reykjanes geothermal system, Iceland: evidence from Iceland Deep Drilling Project core RN-17B. *J. Volcanol. Geoth. Res.* **302**, 47–63.

Franzson H., Sigvaldason H., Sigurdsson H. and Agustsson H. (1983) Nesjavellir well NG-7: LIthology and drilling data from 593 to 2001 m, Report prepared for Hitaveita Reykjavikur OS-83105/JHD-41(in Icelandic).

Friðleifsson G. Ó., Albertsson A., Elders W., Sigurdsson Ó., Karlsdóttir R. and Pálsson B. (2011) The Iceland Deep Drilling Project (IDDP): planning for the second deep well at Reykjanes. *Geoth. Resour. Council Trans.* **35**, 347–354.

Friðleifsson G. Ó., Elders W. A., Zierenberg R. A., Stefánsson A., Fowler A. P. G., Weisenberger T. B., Harðarson B. S. and Mesfin K. (2017) The Iceland deep drilling project 4.5km deep well, IDDP-2, in the seawater-recharged Reykjanes geothermal field in SW Iceland has successfully reached its supercritical target. *Sci. Drill.* **23**, 1–12. https://doi.org/10.5194/sd-23-1-2017.

Fridriksson, T., Giroud, N., 2008. Geochemical monitoring of the Reykjanes geothermal field from 2006 to 2007. Report Prepared for Hitaveitu Sudurnesja ISOR-2008/021 (in Icelandic), 51 p.

Friedrichsen H. (1985) Strontium, oxygen, and hydrogen isotope studies on primary and secondary minerals in basalts from the Costa Rica Rift, Deep Sea Drilling Project Hole 504B, Leg 83. Proceedings of the Ocean Drilling Program, Scientific Results, 289–295.

Fujimaki H. (1986) Partition coefficients of Hf, Zr, and REE between zircon, apatite, and liquid. *Contrib. Miner. Petrol.* **94**, 42–45.

Gillis K. M. (2002) The rootzone of an ancient hydrothermal system exposed in the Troodo Ophiolite, Cyprus. *J. Geol.* **110**, 57–74.

Goodfellow W. D. and Franklin J. M. (1993) Geology, mineralogy, and chemistry of sediment-hosted clastic massive sulfides in shallow cores, Middle Valley, Northern Juan De Fuca Ridge. *Econ. Geol.* **88**, 2037–2068.

Gregory R. T. and Taylor H. P. (1981) An oxygen isotope profile in a section of Cretaceous oceanic crust, Samail Ophiolite, Oman: Evidence for δ18O buffering of the oceans by deep (>5 km) seawater-hydrothermal circulation at mid-ocean ridges. *J. Geophys. Res. Solid Earth* **86**, 2737–2755.

Gudmundsson B. T. and Arnórsson S. (2002) Geochemical monitoring of the Krafla and Namafjall geothermal areas, N-Iceland. *Geothermics* **31**, 195–243.

Haas J. R., Shock E. L. and Sassani D. C. (1995) Rare earth elements in hydrothermal systems: estimates of standard partial molal thermodynamic properties of aqueous complexes of the rare earth elements at high pressures and temperatures. *Geochim. Cosmochim. Acta* **59**, 4329–4350.

Hardardóttir V., Brown K. L., Fridriksson T., Hedenquist J. W., Hannington M. D. and Thorhallsson S. (2009) Metals in deep liquid of the Reykjanes geothermal system, southwest Iceland: implications for the composition of seafloor black smoker fluids. *Geology* **37**, 1103–1106.

Hardardóttir V., Ármannsson H. and Þórhallsson S. (2005) Characterization of sulfide-rich scales in brine at Reykjanes. Proceedings World Geothermal Congress 2005, Antalya, Turkey, 24–29 April 2005.

Hardardóttir V., Hannington M., Hedenquist J., Kjarsgaard I. and Hoal K. (2010) Cu-rich scales in the Reykjanes geothermal system, Iceland. *Econ. Geol.* **105**, 1143–1155.

Hardardóttir V., Hannington M. and Hedenquist J. (2013) Metal concentrations and metal deposition in deep geothermal wells at the reykjanes high-temperature area, Iceland. *Procedia Earth Planet. Sci.* **7**, 338–341.

Hardardóttir V. (2002) Scales in well 9 Reykjanes. Report OS-2002-11, 47 pages (in Icelandic).

Hartanto, D.B., 2005. Borehole geology and alteration mineralogy of well HE-11. Hellisheidi geothermal field, SW-Iceland. UNU-GTP Report 8, 83–109.

Henley R. W. (1984) Chemical structure of geothermal systems. In Fluid-mineral equilibria in hydrothermal systems (eds. Robertson J.M.). Reviews in Economic Geology 1, 9–28.

Humphris S. E. and Bach W. (2005) On the Sr isotope and REE compositions of anhydrites from the TAG seafloor hydrothermal system. *Geochim. Cosmochim. Acta* **69**, 1511–1525.

Jakobsson S. P., Jonsson J. and Shido F. (1978) Petrology of the western Reykjanes Peninsula, Iceland. *J. Petrol.* **19**, 669–705.

James R. H., Elderfield H. and Plamer M. R. (1995) The chemistry of hydrothermal fluids from the Broken Spur site, 29N Mid-Atlantic Ridge. *Geochim. Cosmochim. Acta* **59**, 651–659.

Janots E., Brunet F., Goffé B., Poinssot C., Burchard M. and Cemič L. (2007) Thermochemistry of monazite-(La) and dissakisite-(La): implications for monazite and allanite stability in metapelites. *Contrib. Miner. Petrol.* **154**, 1–14.

Kaasalainen H. and Stefánsson A. (2012) The chemistry of trace elements in surface geothermal waters and steam, Iceland. *Chem. Geol.* **330–331**, 60–85.

Kaasalainen H., Stefánsson A., Giroud N. and Arnórsson S. (2015) The geochemistry of trace elements in geothermal fluids, Iceland. *Appl. Geochem.* **62**, 207–223.

Kawahata H., Kusakabe M. and Kikuchi Y. (1987) Strontium, oxygen, and hydrogen isotope geochemistry of hydrothermally altered and weathered rocks in DSDP Hole 504B, Costa Rica Rift. *Earth Planet. Sci. Lett.* **85**, 343–355.

Kewiy, W.R., 2013. Injection and production well testing in the geothermal fields of southern Hengill and Reykjanes, SW-Iceland and Theistareykir, N-Iceland. Geothermal Training in Iceland 2013, UNU-GTP, Iceland, 747–768.

Kikawada Y., Oi T., Ossaka T., Kakihana H. and Honda T. (1995) Leaching of lanthanoids from andesitic rocks by acidic aqueous solutions. *Geochem. J.* **29**, 67–84.

Kirchner T. M. and Gillis K. M. (2012) Mineralogical and strontium isotopic record of hydrothermal processes in the lower ocean crust at and near the East Pacific Rise. *Contrib. Miner. Petrol.* **164**, 123–141.

Klinkhammer G. P., German C. R., Elderfield H., Greaves M. J. and Mitra A. (1994) Rare earth elements in hydrothermal fluids and plume particulates by inductively coupled plasma mass spectrometry. *Mar. Chem.* **45**, 179–186.

Kristmannsdóttir H. (1989) Types of scaling occurring by geothermal utilization in Iceland. *Geothermics* **18**, 183–190.

Lawrence M. G. and Kamber B. S. (2007) Rare earth element concentrations in the natural water reference materials (NRCC) NASS-5, CASS-4 and SLEW-3. *Geostand. Geoanal. Res.* **31**, 95–103.

Lemaitre N., Bayon G., Ondréas H., Caprais J.-C., Freslon N., Bollinger C., Rouget M.-L., de Prunelé A., Ruffine L., Olu-Le Roy K. and Sarthou G. (2014) Trace element behaviour at cold seeps and the potential export of dissolved iron to the ocean. *Earth Planet. Sci. Lett.* **404**, 376–388.

Lewis A. J., Komninou A., Yardley B. W. D. and Palmer M. R. (1998) Rare earth element speciation in geothermal fluids from Yellowstone National Park, Wyoming, USA. *Geochim. Cosmochim. Acta* **62**, 657–663.

Libbey R. B. and Williams-Jones A. E. (2016) Relating sulfide mineral zonation and trace element chemistry to subsurface processes in the Reykjanes geothermal system, Iceland. *J. Volcanol. Geoth. Res.* **310**, 225–241.

Lindal B. (1989) Solids deposition in view of geothermal applications in Reykjanes and Svartsengi, south western Iceland. *Geothermics* **18**, 207–216.

Liu W., Etschmann B., Migdisov A., Boukhalfa H., Testemale D., Müller H., Hazemann J.-L. and Brugger J. (2017) Revisiting the hydrothermal geochemistry of europium(II/III) in light of new in-situ XAS spectroscopy results. *Chem. Geol.* **459**, 61–74.

Lonker S. W., Franzson H. and Kristmannsdóttir H. (1993) Mineral fluid interactions in the Reykjanes and Svartsengi geothermal systems. *Am. J. Sci.* **293**, 605–670.

Lottermoser B. G. (1992) Rare earth elements and hydrothermal ore formation processes. *Ore Geol. Rev.* **7**, 25–41.

Marks N., Schiffman P., Zierenberg R., Franzson H. and Friðleifsson G. Ó. (2010) Hydrothermal alteration in the Reykjanes geothermal system: Insights from Iceland deep drilling program well RN-17. *J. Volcanol. Geoth. Res.* **189**, 172–190.

Marks N., Zierenberg R. A. and Schiffman P. (2015) Strontium and oxygen isotopic profiles through 3km of hydrothermally altered oceanic crust in the Reykjanes Geothermal System, Iceland. *Chem. Geol.* **412**, 34–47.

McDonough W. F. and Sun S. S. (1995) The composition of the Earth. *Chem. Geol.* **120**, 223–253.

McLennan S. M. (1989) Rare earth elments in sedimentary rocks: Influence of provenance and sedimentary processes. *Rev. Mineral.* **21**, 169–200.

Meier D. B., Gunnlaugsson E., Gunnarsson I., Jamtveit B., Peacock C. L. and Benning L. G. (2014) Microstructural and chemical variation in silica-rich precipitates at the Hellisheiði geothermal power plant. *Mineral. Mag.* **78**, 1381–1389.

Michard G., Albarede F., Michard A., Minster J. F., Charlou J. L. and Tan N. (1984) Chemistry of solutions from the 13°N East Pacific Rise hydrothermal site. *Earth Planet. Sci. Lett.* **67**, 297–307.

Michard A. and Albaréde F. (1986) The REE content of some hydrothermal fluids. *Chem. Geol.* **55**, 51–60.

Michard A., Albaréde F., Michard G., Minster J. F. and Charlou J. L. (1983) Rare-earth elements and uranium in high temperature solutions from East Pacific Rise hydrothermal vent field. *Nature* **303**, 795–797.

Migdisov A. A. and Williams-Jones A. E. (2008) A spectrophotometric study of Nd(III), Sm(III) and Er(III) complexation in sulfate-bearing solutions at elevated temperatures. *Geochim. Cosmochim. Acta* **72**, 5291–5303.

Migdisov A. A., Williams-Jones A. E. and Wagner T. (2009) An experimental study of the solubility and speciation of the Rare Earth Elements (III) in fluoride- and chloride-bearing aqueous solutions at temperatures up to 300 °C. *Geochim. Cosmochim. Acta* **73**, 7087–7109.

Migdisov A. A. and Williams-Jones A. E. (2014) Hydrothermal transport and deposition of the rare earth elements by fluorine-bearing aqueous liquids. *Miner. Deposita* **49**, 987–997.

Migdisov A., Williams-Jones A. E., Brugger J. and Caporuscio F. A. (2016) Hydrothermal transport, deposition, and fractionation of the REE: experimental data and thermodynamic calculations. *Chem. Geol.* **439**, 13–42.

Mitra A., Elderfield H. and Greaves M. J. (1994) Rare earth elements in submarine hydrothermal fluids and plumes from the Mid-Atlantic Ridge. *Mar. Chem.* **46**, 217–235.

Möller P., Dulski P. and Morteani G. (2003) Partitioning of rare earth elements, yttrium, and some major elements among source rocks, liquid and vapor of Larderello-Travale Geothermal Field, Tuscany (Central Italy). *Geochim. Cosmochim. Acta* **67**, 171–183.

Möller P., Dulski P. and Özgür N. (2008) Partitioning of rare earths and some major elements in the Kizildere geothermal field, Turkey. *Geothermics* **37**, 132–156.

Moore R. B. and Truesdell F. A. (1993) Geology of Kiluea volcano. *Geothermics* **22**, 243–254.

Nehlig P., Juteau T., Bendel V. and Cotten J. (1994) The root zones of oceanic hydrothermal systems: constraints from the Samail ophiolite (Oman). *J. Geophys. Res. Solid Earth* **99**, 4703–4713.

Novak E. A. and Evans S. R. (1991) Preliminary results from two scientific observation holes on the Kilauea East Rift Zone. *Geoth. Resour. Counc. Trans.* **15**, 187–192.

Palandri, J., Reed, M., 2016. SOLTHERM.xpt: Thermodynamic and related data for programs SOLVEQ-XPT, CHIM-XPT, and GEOCAL-XPT. <http://pages.uoregon.edu/palandri/data/soltherm.REE_working.xpt> (Last accessed 7.12.2018).

Pan Y. and Fleet M. E. (2002) Compositions of the apatite-group minerals: substitution mechanisms and controlling factors. *Rev. Mineral. Geochem.* **48**, 13–49.

Pang Z. H. and Reed M. (1998) Theoretical chemical thermometry on geothermal water: problems and methods. *Geochimica et Cosmochimica Acta* **62**, 1083–1091.

Quane S. L., Garcia M. O., Guillou H. and Hulsebosch T. P. (2000) Magmatic history of the East Rift Zone of Kilauea Volcano, Hawaii based on drill core from SOH 1. *J. Volcanol. Geoth. Res.* **102**, 319–338.

Ragnarsdóttir K. V., Walther J. V. and Arnórsson S. (1984) Description and interpretation of the composition of fluid and alteration mineralogy in the geothermal system, at Svartsengi, Iceland. *Geochimica et Cosmochimica Acta* **48**, 1535–1553.

Reed M. (1982) Calculation of multicomponent chemcial equilibria and reaction processes in systems involving minerals, gases and an aqueous phase. *Geochim. Cosmochim. Acta* **46**, 513–528.

Reed M., Spycher N. and Palandri J. (2016a) SOLVEQ-XPT: A computer program for computing aqueous-mineral-gas equilibria. University of Oregon Department of Geological Sciences, Eugene, Oregon, 41 p.

Reed M., Spycher N. and Palandri J. (2016b) Users guide for CHIM-XPT: a program for computing reaction processes in aqueous-mineral-gas systems and MINTAB guide. University of Oregon Department of Geological Sciences, Eugene, Oregon, 71 p., Department of Geological Sciences, University of Oregon, Eugene, Oregon, USA.

Reed M. and Spycher N. (1984) Calculation of pH and mineral equilibria in hydrothermal waters with application to geothermometry and studies of boiling and dilution. *Geochimica et Cosmochimica Acta* **48**, 1479–1492.

Reynard B., Lécuyer C. and Grandjean P. (1999) Crystal-chemical controls on rare-earth element concentrations in fossil biogenic apatites and implications for paleoenvironmental reconstructions. *Chem. Geol.* **155**, 233–241.

Richardson C. J., Cann J. R., Richards H. G. and Cowan J. G. (1987) Metal-depleted root zones of the Troodos ore-forming hydrothermal systems, Cyprus. *Earth Planet. Sci. Lett.* **84**, 243–253.

Robie R. A., Hemingway B. S. and Fisher J. R. (1978) Thermodynamic properties of minerals and related substances at 298.15K and 1 bar (10^5 pascals) and at higher temperatures. *USGS Bull.* **1452**, 1–456.

Robie R. A. and Hemingway B. S. (1995) Thermodynamic properties of minerals and related substances at 298.15 K and 1 bar (10^5 pascals) and at higher temperatures. *USGS Bull.* **2131**, 1–461.

Sæmundsson K. (1979) Outline of the geology of Iceland. *Jökull* **29**, 7–28.

Sanada T., Takamatsu N. and Yoshiike Y. (2006) Geochemical interpretation of long-term variations in rare earth element concentrations in acidic hot spring waters from the Tamagawa geothermal area, Japan. *Geothermics* **35**, 141–155.

Schiffman P. and Friðleifsson G. Ó. (1991) The smectite-chlorite transition in drillhole N 1–15, Nesjavellir geothermal field, Iceland – XRD, BSE and electron microprobe investigations. *J. Metamorph. Geol.* **9**, 679–696.

Schmidt K., Garbe-Schönberg D., Bau M. and Koschinsky A. (2010) Rare earth element distribution in >400 °C hot hydrothermal fluids from 5°S, MAR: the role of anhydrite in controlling highly variable distribution patterns. *Geochimica et Cosmochimica Acta* **74**, 4058–4077.

Seyfried Jr, W.E. and Ding, K. (1993b) Phase equilibria in subseafloor hydrothermal systems: a review of the role of redox, temperature, Ph and dissolved Cl on the chemistry of hot spring fluids at mid-ocean ridges. In Seafloor Hydrothermal Systems: Physical, Chemical, Biological, and Geological Interactions. American Geophysical Union, pp 248–272. 248–272.

Seyfried, Jr, W. E. and Bischoff J. L. (1977) Hydrothermal transport of heavy metals by seawater: The role of seawater/basat ratio. *Earth Planet. Sci. Lett.* **34**, 71–77.

Seyfried, Jr, W. E. and Ding K. (1993) The effect of redox on the relative solubilities of copper and iron in Cl-bearing aqueous fluids at elevated temperatures and pressures – an experimental study with application to subseafloor hydrothermal systems. *Geochim. Cosmochim. Acta* **57**, 1905–1917.

Shibata S.-N., Tanaka T. and Yamamoto K. (2006) Crystal structure control of the dissolution of rare earth elments in water-mineral interactions. *Geochem. J.* **40**, 437–446.

Shock E. L. and Helgeson H. C. (1988) Calculation of the thermodynamic and transport properties of aqueous species at high pressures and temperatures: correlation algorithms for ionic species and equation of state predictions to 5 kb and 1000 °C. *Geochim. Cosmochim. Acta* **52**, 2009–2036.

Shock E. L., Sassini D., Willis M. and Sverjensky D. (1997) Inorganic species in geologic fluids: correlations among standard molal thermodynamic properties of aqueous ions and hydroxide complexes. *Geochimica et Cosmochimica Acta* **61**, 907–950.

Sorey, M.L., Colvard, E.M., 1994. Potential effects of the Hawaii geothermal project on groundwater resources on the island of Hawaii. U.S. Geological Survey Water Resources Investigations Report 94-4028, Menlo Park, California.

Spear F. S. (2010) Monazite–allanite phase relations in metapelites. *Chem. Geol.* **279**, 55–62.

Spear F. S. and Pyle J. M. (2002) Apatite, monazite, and xenotime in metamorphic rocks. *Rev. Mineral. Geochem.* **48**, 293–335.

Spooner E. T. C., Chapman H. J. and Smewing J. D. (1977) Strontium isotopic contamination and oxidation during ocean floor hydrothermal metamorphism of the ophiolitic rocks of the Troodos Massif, Cyprus. *Geochim. Cosmochim. Acta* **41**, 873–890.

Spycher N. F. and Reed M. H. (1989) Evolution of a Broadlands-type epithermal ore fluid along alternative P-T paths: implications for the transport and deposition of base, precious, and volatile metals. *Econ. Geol.* **8**, 328–359.

Stefánsson, A., Gunnlaugsson, E., 1985. Nesjavellir well NG-7 warm up and production testing. Report Prepared for Hitaveitu Reykjavikur OS-85035/JHD-11 (in Icelandic).

Stefánsson A. and Arnórsson S. (2002) Gas pressures and redox reactions in geothermal fluids in Iceland. *Chem. Geol.* **190**, 251–271.

Steingrimsson, B., Thordarson, S., 2001. Measurement and monitoring during 1998-2000 at Nesjavellir, Kolviðarhóll and Ölkelduháls. Report prepared for Orkuveitu Reykjavikur. OS-2001-033 (in Icelandic), 2001, 56 p.

Stone C. and Fan P.-F. (1978) Hydrothermal alteration of basalts from Hawaii Geothermal Project Well-A, Kilauea. *Hawaii Geology* **6**, 401–404.

Sverjensky D. (1984) Europium redox equilibria in aqueous solutions. *Earth Planet. Sci. Lett.* **67**, 70–78.

Tareke, F., 2002. Evaluation of wellbore parameters for well HE-4, Hellisheidi, SW-Iceland. UNU-GTP Report 14, 265–286.

Tomasson J. and Kristmannsdóttir H. (1972) High temperature alteration minerals and thermal brines, Reykjanes, Iceland. *Contrib. Miner. Petrol.* **36**, 123–134.

van Middlesworth P. E. and Wood S. (1997) The aqueous geochemistry of the rare earth elements and yttrium. Part 7. REE, Th and U contents in thermal springs associated with the Idaho batholith. *Appl. Geochem.* **13**, 861–884.

Von Damm K. L., Edmond J. M., Grant B., Measures C. I., Walden B. and Weiss R. F. (1985) Chemistry of submarine hydrothermal solutions at 21 N East Pacific Rise. *Geochim. Cosmochim. Acta* **49**, 2197–2220.

Von Damm K. L., Lilley M. D., Shanks W. C., Brockington M., Bray A. M., O'Grady K. M., Olson E., Graham A. and Proskurowski G. (2003) Extraordinary phase separation and segregation in vent fluids from the East Pacific Rise. *Earth Planet. Sci. Lett.* **206**, 365–378.

Wagner W. and Kretschmar H.J. (2008) International steam tables, properties of water and steam based on the industrial formulation IAPWS-IF97, 2nd ed, p 392. Springer-Verlag, Berlin, Heidelberg.

Wang B. S., Lee C. P. and Ho T. Y. (2014) Trace metal determination in natural waters by automated solid phase extraction system and ICP-MS: the influence of low level Mg and Ca. *Talanta* **128**, 337–344.

West H. B., Delanoy G. A., Thomas D. M., Gerlach D. C., Chen B., Takahashi P. and Thomas D. M. (1992) Trace element and isotope geochemistry of geothermal fluids, East Rift Zone, Kilauea, Hawaii. No. DOE/SF/15799-T14. Hawaii Univ., Honolulu, HI (United States).

Wheat C. G., Feely R. A. and Mottl M. J. (1996) Phosphate removal by oceanic hydrothermal processes: an update of the phosphorus budget in the oceans. *Geochimica et Cosmochimica Acta* **60**, 3593–3608.

Wheat C. G., Mottl M. J. and Rudnicki M. (2002) Trace element and REE composition of a low-temperature ridge-flank hydrothermal spring. *Geochimica et Cosmochimica Acta* **66**, 3693–3705.

Williams-Jones A. E., Migdisov A. A. and Samson I. M. (2012) Hydrothermal mobilization of the Rare Earth Elements – A tale of "Ceria" and "Yttria". *Elements* **8**, 355–360.

Wood S. A., Palmer D. A., Wesolowski D. J. and Bénézeth P. (2002) The aqueous geochemistry of the rare earth elements and yttrium. Part XI. The solubility of Nd(OH)2 and hydrolysis of Nd3+ from 30 to 290 °C at saturated water vapor pressure with in-situ pH measurements. Water-rock Interactions, Ore Deposits and Environmental Geochemistry: A tribute to David A. Crerar (eds R. Hellman and S.A. Wood) 7, 229–256.

Zhu Y., Itoh A., Fujimori E., Umemura T. and Haraguchi H. (2006) Determination of rare earth elements in seawater by ICP-MS after preconcentration with a chelating resin-packed minicolumn. *J. Alloy. Compd.* **408–412**, 985–988.

Zhu Y., Itoh A., Umemura T., Haraguchi H., Inagaki K. and Chiba K. (2010) Determination of REEs in natural water by ICP-MS with the aid of an automatic column changing system. *J. Anal. At. Spectrom.* **25**, 1253–1258.

Zhu C. and Sverjensky D. A. (1991) Partitioning of F-Cl-OH between minerals and hydrothermal fluids. *Geochimica et Cosmochimica Acta* **55**, 1837–1858.

Zierenberg R. A., Fowler A. P. G. and Friðleifsson G. Ó. (2017) Preliminary description of rocks and alteration in IDDP-2 drill core samples recovered from the Reykjanes geothermal system, Iceland. Geothermal Resources Council Transactions 41.

Zierenberg R., Fouquet Y., Miller D. J., Bahr J. M., Baker P. A., Bjerkgård T., Brunner C. A., Duckworth R. C., Gable R., Gieskes J., Goodfellow W. D., Gröschel-Becker H. M., Guèrin G., Ishibashi J., Iturrino G., James R. H., Lackschewitz K. S., Marquez L. L., Nehlig P., Peter J. M., Rigsby C. A., Schultheiss P., Shanks, III, W. C., Simoneit B. R. T., Summit M., Teagle D. A. H., Urban T. C. and Zuffa G. G. (1998) The deep structure of a sea-floor hydrothermal deposit. *Nature* **392**, 485–488.

Associate editor: Rachael James